Figure 2. Double immunofluorescence staining of Smad2 and β-catenin

From the left to right, panels show nuclear counterstaining with DAPI [1], visualization of Smad2 [2] and β-catenin [3] using Alexa Fluor® 488- and 594-labeled secondary antibodies, respectively, and merged images [4]. Panel A shows normal colonic tissues of AOM-untreated healthy rats, panel B shows tumor tissues from the MSC (-) group, and panel C shows tumor tissues from the MSC Day0 group. White arrowheads in panel B indicate nuclear staining of Smad2. Bar scales at the right lower corner in each panel indicated 10 μm.

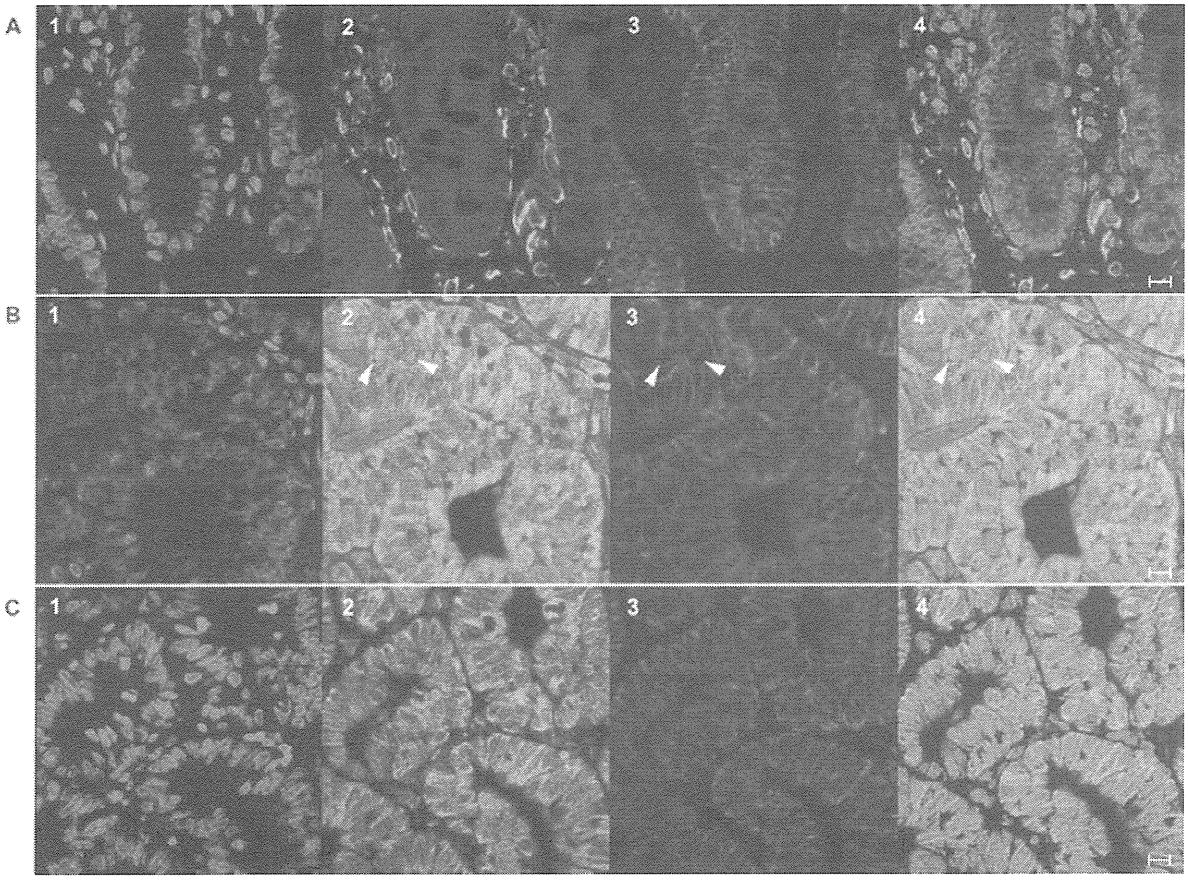

Figure 3. Analysis of the ACF model

ACF model rats (n = 15) were classified into three groups (n = 5 each group) according to the timing of MSC administration either before or after administration of two separate of AOM on Days 0 and 7: MSC (-), MSC pre-AOM (Day–1), and MSC post-AOM (Day 8) groups (A). A total of 400 ACF developed: 213, 95, and 92 in MSC (-), MSC Day–1, and MSC Day8 groups, respectively. The average ACF density is shown in panel B. *1, $P = 4.7E-4$; *2, $P = 0.001$. The average ACF density in the proximal, middle, and distal colon is shown in panel C. *1, $P = 0.02$; *2, $P = 1.6E-4$; *3, $P = 0.037$; *4, $P = 0.017$; *5, $P = 0.022$; *6, $P = 0.002$; *7, $P = 0.004$; *8, $P = 4.0E-5$; *9, $P = 2.2E-4$; *10, $P = 2.1E-7$; *11, $P = 1.9E-6$. Representative ACs, one to more than four ACs per focus, are shown in panels D1–4, respectively. Scale bars: 50 μm. The average density of ACs per focus, one to more than four ACs, is shown in panel E. *1, $P = 0.009$; *2, $P = 0.011$; *3, $P = 5.2E-5$; *4, $P = 7.3E-5$; *5, $P = 0.005$; *6, $P = 7.3E-5$; *7, $P = 5.3E-5$; *8, $P = 1.7E-4$; *9, $P = 7.9E-5$; *10, $P = 0.021$; *11, $P = 0.005$; *12, $P = 4.0E-6$; *13, $P = 6.4E-6$; *14, $P = 0.001$; *15, $P = 0.001$. Panel F shows the analysis of TGF-β signaling by western blotting of Smad2 and phospho-Smad2. Lanes 1–5, 6–10, and 11–15 show data for MSC (-) control MSC Day–1, and MSC Day8 groups, respectively.

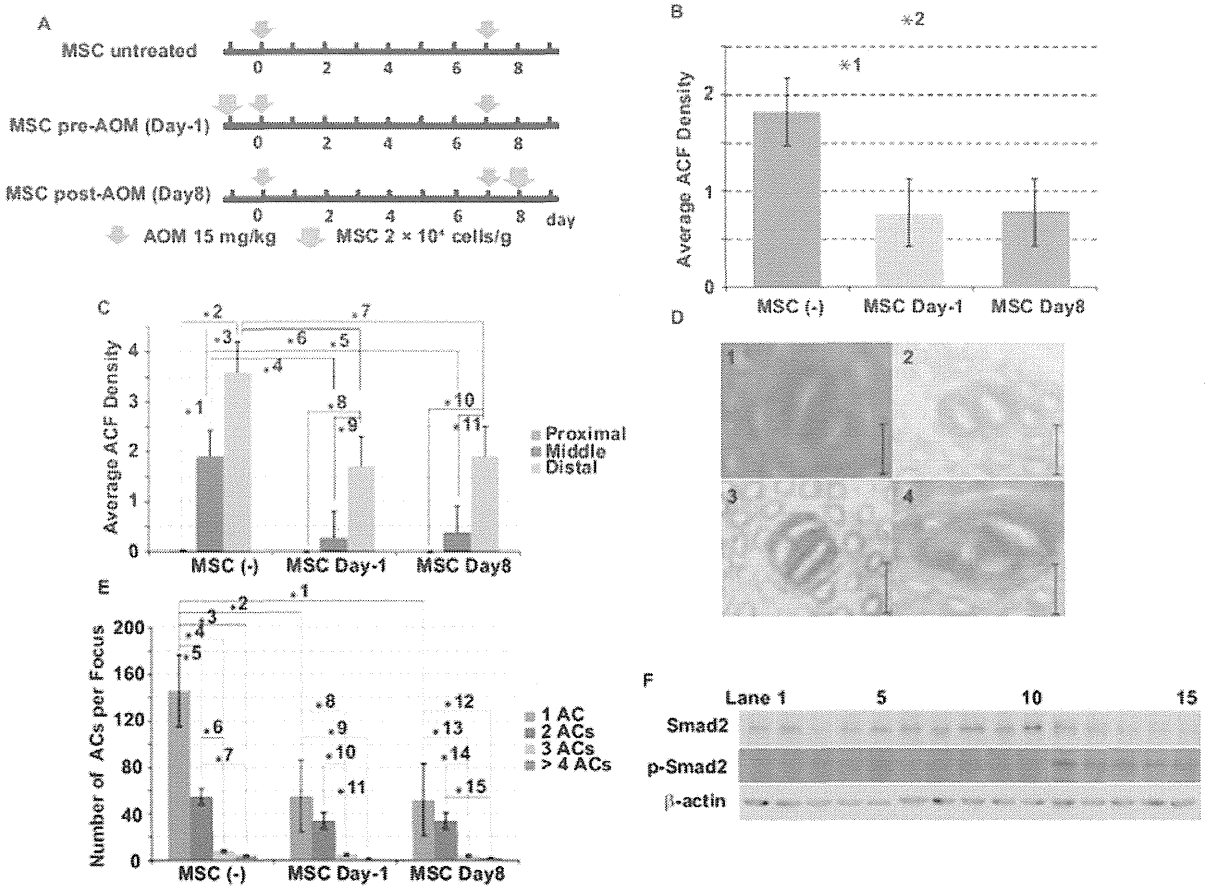

Figure 4. Effects of MSCs on the AARGC

AARGC model rats (n = 15) were classified into five groups (n = 5 each group) according to the treatment at 24 h before administration of a single dose of AOM on Day 0: MSC (-) control (PBS), MSC, HSC, 3Y1, and MSC-CM groups. Rats were sacrificed at 0 h when AOM was intraperitoneally injected at 4, 8, 16, 24, and 48 h for subsequent analyses (A). Representative TUNEL immunostaining is shown for control (upper) and MSC-24h groups (lower) at 8 h. The right panel shows magnified views corresponding to the rectangles in the left panel (B). Bar scales at the right lower corner in each panel indicated 250 μm. The apoptotic index was calculated as the percentage of positive nuclear immunostaining of TUNEL reactions in approximately 1,000 crypt epithelial cells at each indicated time point (C). *MSC *vs.* control, $P = 0.006$; MSC *vs.* HSC, $P = 2.9E\text{-}4$; MSC *vs.* 3Y1, $P = 0.001$; MSC *vs.* MSC-CM, $P = 1.7E\text{-}4$: **MSC *vs.* HSC, $P = 0.010$; MSC *vs.* 3Y1, $P = 0.005$; MSC *vs.* MSC-CM $P = 1.3E\text{-}5$. Representative Ki-67 immunofluorescence in shown for control (left) and MSC groups (right) at 4 h (D). Bar scales at the right lower corner in each panel indicated 10 μm. The Ki-67 labeling index was calculated as the percentage of positive nuclear immunofluorescence in approximately 1,000 epithelial cells at each indicated time point (E). *MSC *vs.* control, $P = 0.037$: **MSC *vs.* control, $P = 2.2E\text{-}4$; MSC *vs.* HSC, $P = 3.2E\text{-}5$; MSC *vs.* 3Y1, $P = 0.002$. Ki-67 immunofluorescence and TUNEL reactions were performed using at least five different specimens in triplicate. Western blot analyses of Akt and MAP kinase signaling between MSC-treated and MSC-untreated control groups was performed (F).

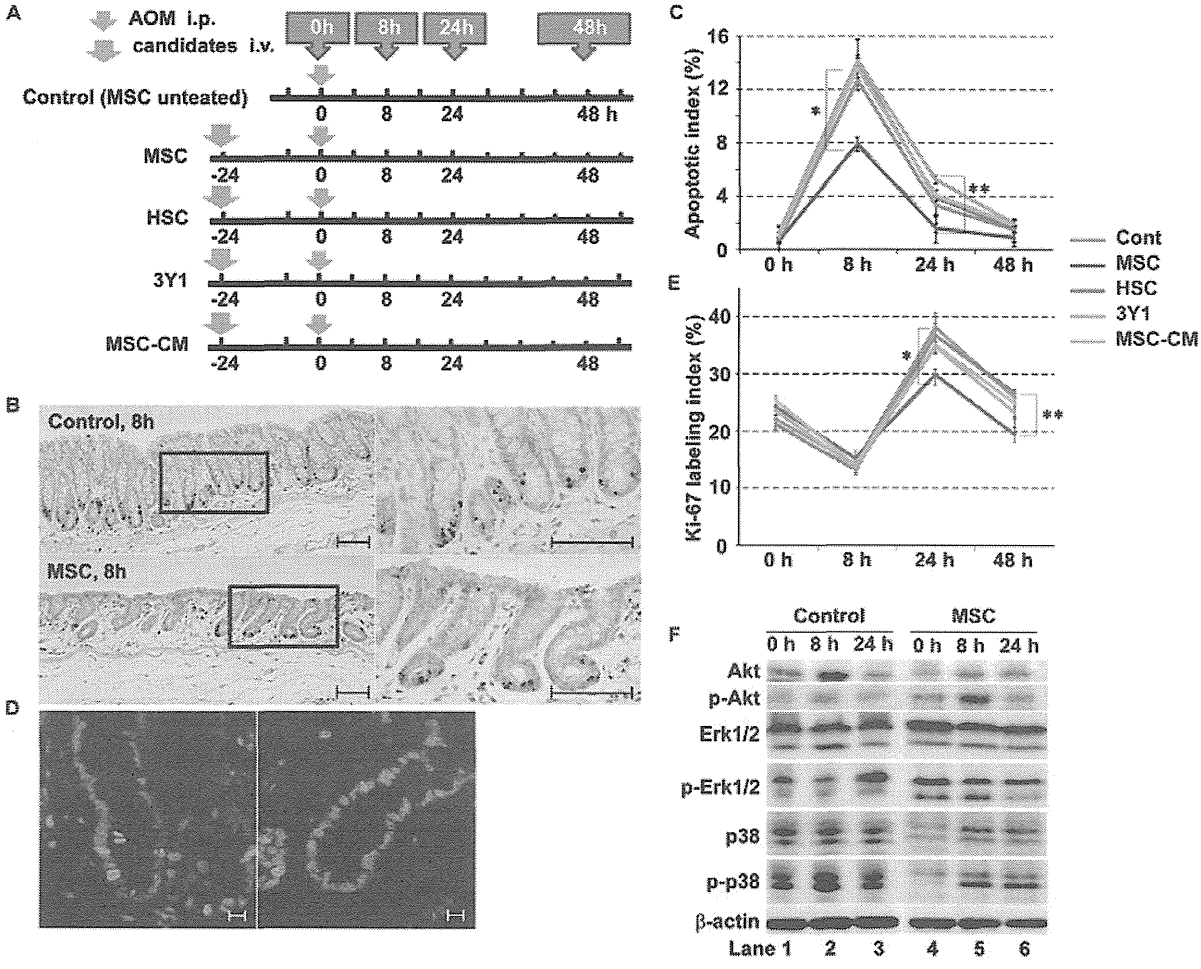
A
AOM i.p.
candidates i.v.
0h
8h
24h
48h
Control (MSC unteated)
0 8 24 48 h
MSC
-24 0 8 24 48
HSC
-24 0 8 24 48
3Y1
-24 0 8 24 48
MSC-CM
-24 0 8 24 48
B
Control, 8h
MSC, 8h
C
Apoptotic index (%)
16
12
8
4
0
0 h 8 h 24 h 48 h
Cont
MSC
HSC
3Y1
MSC-CM
D
E
Ki-67 labeling index (%)
40
30
20
10
0
0 h 8 h 24 h 48 h
F
Control
MSC
0 h 8 h 24 h 0 h 8 h 24 h
Akt
p-Akt
Erk1/2
p-Erk1/2
p38
p-p38
β-actin
Lane 1 2 3 4 5 6

Figure 5. Mechanistic insight into the suppression of AOM-induced tumor initiation *in vivo*

The results of the *in vivo* immunofluorescence analysis of O^6MeG are depicted in panels A–C. The left panels show nuclei stained with DAPI, the middle panels visualize O^6MeG adducts in nuclear DNA using an Alexa Fluor® 594-labeled secondary antibody, and the right panels are merged images of the left and middle panels in the same row. Panel A shows data from rats sacrificed at 8 h after AOM administration in the MSC (-) control group of the AARGC model, panel B shows data from rats sacrificed at 8 h after AOM administration in the MSC-24h group, and panel C shows data from AOM-untreated healthy rats. Bar scales at the right lower corner in each panel indicated 10 μm. In panel D, relative expression of *Mgmt* in the mucosa was evaluated by qPCR. *1, $P = 0.021$; *2, $P = 0.018$. Panel E shows the results of western blot analyses of Smad2, phospho-Smad2, IKKβ, IκBα, Bcl-2, Bcl-xL, cIAP-2, p21, Bax, Cdk4, Rb, and phospho-Rb. Lanes 1–5 correspond to 0–24 h, and the left and right panels correspond to the control and MSC-24h groups, respectively. The data are representative of three independent experiments.

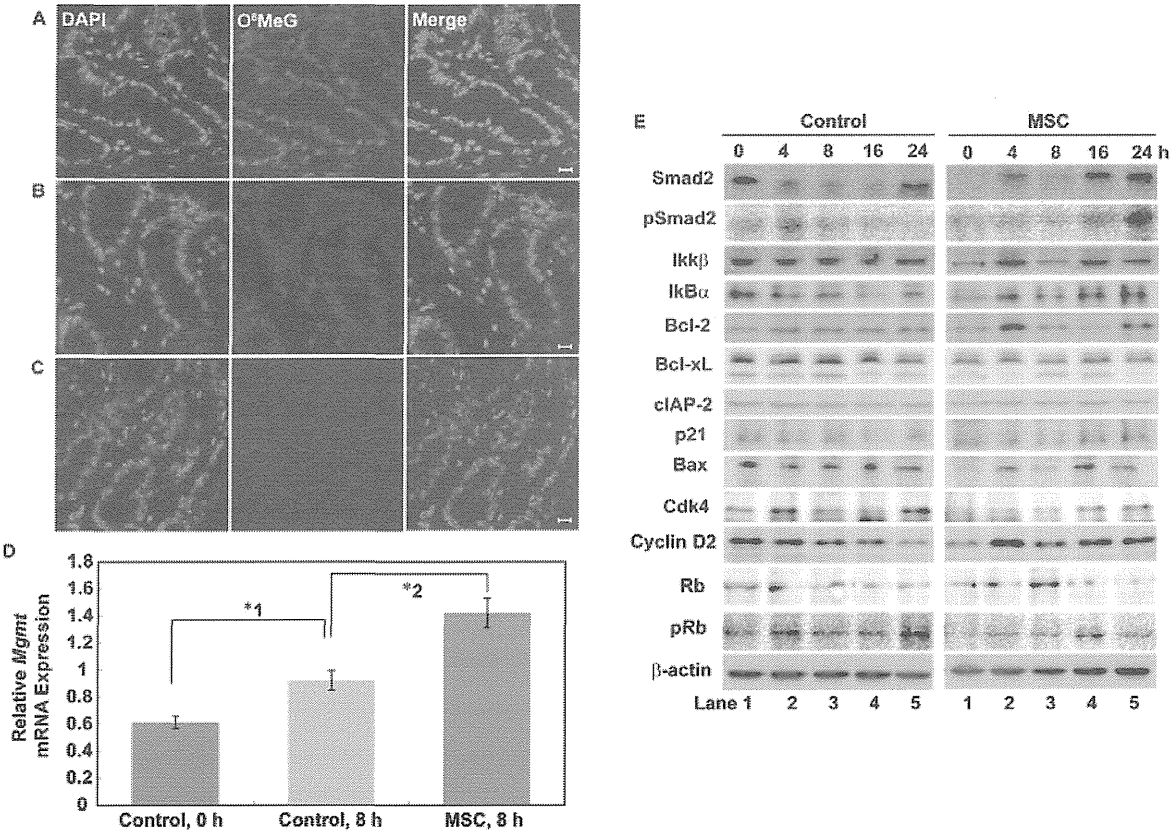

Figure 6. Mechanistic insight into suppression of AOM-induced tumor initiation *in vitro*

The Ki-67 labeling index was calculated in triplicate and bar charts were constructed for the following conditions: IEC-6 cells treated with AOM cocultured with or without MSCs, IEC-6 cells treated with MAM cocultured with or without MSCs, IEC-6 cells treated with AOM and O^6BG cocultured with or without MSCs, and IEC-6 cells treated with MAM and O^6BG cocultured with or without MSC (A). *1, $P = 4.0E-4$; *2, $P = 4.0E-4$; *3, $P = 4.0E-4$; *4, $P = 4.0E-4$; *5, $P = 4.0E-4$; *6, $P = 4.0E-4$; *7, $P = 4.0E-4$; *8, $P = 4.0E-4$; *9, $P = 4.0E-4$; *10, $P = 4.0E-4$; *11, $P = 4.0E-4$. The apoptotic index of IEC-6 cells was calculated based on TUNEL staining in triplicate and bar charts were constructed for the conditions described above (B). Representative Ki-67 immunofluorescence of IEC-6 cells (C) and IEC-6 cell cocultures in which cells emitting green fluorescence are GFP-labeled MSCs (D). Cell culture images were taken at a magnifying power of 630. The cell cycle of cocultured IEC-6 cells was analyzed by flow cytometry at 24 h (left), 48 h (middle), and 72 h (right) in triplicate (E). IEC-6 proliferation was assayed by MTT for the following groups in triplicate: without AOM, cocultured with MSCs (direct), cocultured with MSCs (indirect), treated with MSC-CM, and cocultured directly with MSCs and treated with anti-TGF-β neutralizing antibodies (F).

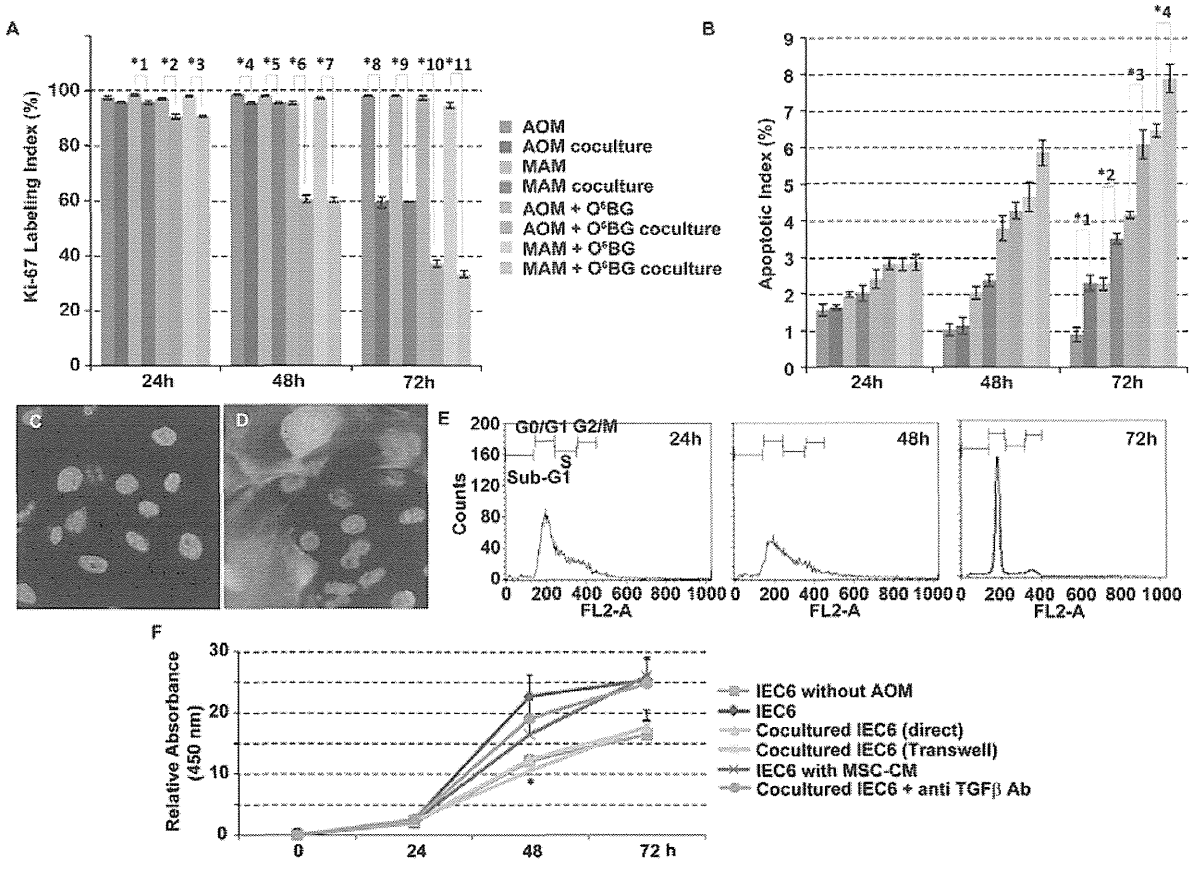

Figure 7. The tandem mechanisms of MSC chemoprevention involved in AOM-induced tumor initiation

The first mechanism of chemoprevention is an indirect measure exerted by MSCs: MSCs activate Mgmt in an unknown manner, resulting in suppression of the AARGC because of a reduction of initiating cells harboring O^6MeG adducts. The second mechanism is a direct measure: MSCs induce G1 arrest in early initiated cells evading the AARGC.

Abbreviations: AOM, azoxymethane; MAM, methylazoxymethanol; O^6MeG, O6-methylguanine.

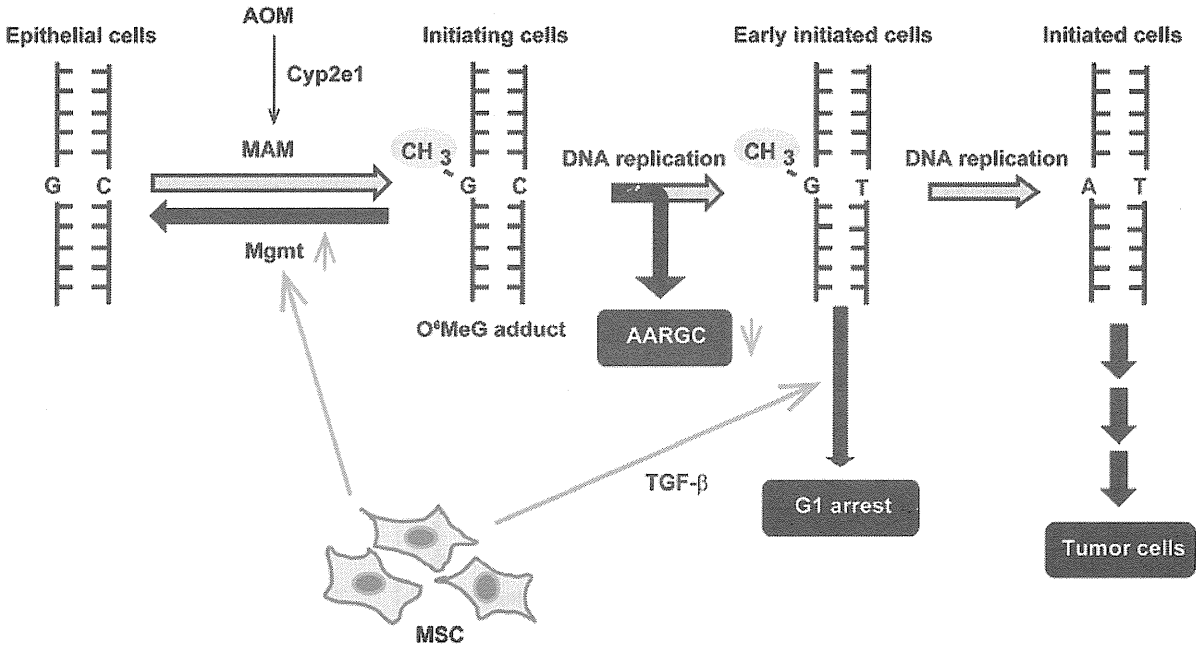

Oncogene (2013), 1–10

www.nature.com/onc

ORIGINAL ARTICLE

microRNA-18a induces apoptosis in colon cancer cells via the autophagolysosomal degradation of oncogenic heterogeneous nuclear ribonucleoprotein A1

M Fujiya[1], H Konishi[1], MK Mohamed Kamel[1], N Ueno, Y Inaba, K Moriichi, H Tanabe, K Ikuta, T Ohtake and Y Kohgo

It is well known that microRNAs (miRs) are abnormally expressed in various cancers and target the messenger RNAs (mRNAs) of cancer-associated genes. While (miRs) are abnormally expressed in various cancers, whether miRs directly target oncogenic proteins is unknown. The present study investigated the inhibitory effects of miR-18a on colon cancer progression, which was considered to be mediated through its direct binding and degradation of heterogeneous nuclear ribonucleoprotein A1 (hnRNP A1). An MTT assay and xenograft model demonstrated that the transfection of miR-18a induced apoptosis in SW620 cells. A binding assay revealed direct binding between miR-18a and hnRNP A1 in the cytoplasm of SW620 cells, which inhibited the oncogenic functions of hnRNP A1. A competitor RNA, which included the complementary sequence of the region of the miR-18a-hnRNP A1 binding site, repressed the effects of miR-18a on the induction of cancer cell apoptosis. *In vitro* single and *in vivo* double isotope assays demonstrated that miR-18a induced the degradation of hnRNP A1. An immunocytochemical study of hnRNP A1 and LC3-II and the inhibition of autophagy by 3-methyladenine and ATG7, p62 and BAG3 siRNA showed that miR-18a and hnRNP A1 formed a complex that was degraded through the autophagolysosomal pathway. This is the first report showing a novel function of a miR in the autophagolysosomal degradation of an oncogenic protein resulting from the creation of a complex consisting of the miR and a RNA-binding protein, which suppressed cancer progression.

Oncogene advance online publication, 28 October 2013; doi:10.1038/onc.2013.429

Keywords: microRNAs; heterogeneous nuclear ribonucleoproteins; colon cancer; apoptosis; autophagy; ubiquitin

INTRODUCTION

Colon cancer is one of the most common causes of cancer-related death in both eastern and western countries. The etiology of colon cancer is associated with genetic and epigenetic abnormalities, including mutations of the *k-ras*, *p53* and *Apc* genes, as well as hypermethylation of the *p16* and *DNA mismatch repair* genes.[1–5] Conversely, recent studies have proposed that, in addition to these DNA abnormalities, the abnormal expression of non-coding RNAs, which account for 97% of all non-ribosomal RNAs in eukaryotes, is also involved in the pathogenesis of tumors.[6] Non-coding RNAs do not code for amino acid sequences, but instead post-transcriptionally regulate the expression of proteins.[7] MicroRNA (miR) are a type of Non-coding RNAs, are short (20–23-nucleotide), endogenous and single-stranded RNA sequences found in almost all eukaryotic cells.[8,9] miRs bind to messenger RNAs (mRNAs) based on their sequence complementarity and regulate the translation of target mRNAs.[10–14] Some miRs, including miR-15 and -16, let-7 and the miR-17-92 cluster,[15–18] are abnormally expressed in tumor cells in various organs, including the colon, and function as suppressors or enhancers of tumor progression. It is thought that miRs regulate the translation of the mRNAs of tumor-related proteins by binding to the mRNAs, as exemplified by the downregulation of MYC by let-7a in lymphoma cells[19] and let-7a in hepatocellular carcinoma and breast cancer cells.[20,21] The targets of each miR appear to be dependent on the organ and histological type of cancer.

miR-18a is highly expressed in several cancer cell types and is thought to be a tumor suppressor.[20,22] The targets of miR-18a have been reported to be the mRNAs of the estrogen receptors in hepatocellular carcinoma[20] and dicer in bladder cancer.[22] However, the target of miR-18a in colon cancer has not been identified, although miR-18a is highly expressed in colon cancer cells.[23]

Conversely, a recent investigation proposed that miR may regulate the protein function without modifying the translation of the mRNA.[24] The authors of that study showed that miR-328 directly binds to heterogeneous nuclear ribonucleoprotein (hnRNP) E2, an RNA binding protein, and inhibits the function of hnRNP E2, leading to the destabilization of the mRNA for CCAAT/enhancer-binding protein alpha in leukemic blasts. This suggests that miRs can inhibit the function of target proteins, particularly RNA-binding proteins (such as those of the hnRNP family), by directly binding to the proteins without influencing the translation of the mRNA. However, the role of the direct binding between proteins and miRs on the physiological function of cells is unclear. We hypothesized that some miRs inhibit the progression of cancer cells by directly binding to RNA-binding proteins, such as hnRNPs, which possess oncogenic properties, and inducing the degradation of these proteins.

This study demonstrates that miR-18a induces the apoptosis of colon cancer cells by directly binding to oncogenic hnRNP A1,which has a binding site for miR-18a[25,26] and leads to the evasion of cancer cell apoptosis, followed by the autophagolysosomal degradation of the protein.

Division of Gastroenterology and Hematology/Oncology, Department of Medicine, Asahikawa Medical College, Asahikawa, Japan. Correspondence: Dr M Fujiya, Division of Gastroenterology and Hematology/Oncology, Department of Medicine, Asahikawa Medical College, 2-1 Midorigaoka-higashi, Asahikawa, Hokkaido 078-8510, Japan.
E-mail: fjym@asahikawa-med.ac.jp
[1]These authors contributed equally to this work.
Received 24 January 2013; revised 12 August 2013; accepted 26 August 2013

RESULTS

Overexpression of miR-18a induces the apoptosis of colon cancer cells

A real-time PCR analysis showed that miR-18a is endogenously expressed in human colon cancer tissues (Supplementary Figure 1A) as well as all colon cancer cell lines examined, including Caco2/bbe, HT29, HCT-116, SKCO-1, SW480 and -620 cells (Supplementary Figure 1B). Double-stranded miR-18a was transfected into colon cancer cell lines to examine the effects of the overexpression of miR-18a on colon cancer progression. A significant augmentation of the miR-18a expression was detected in all cell lines, particularly in the SW620 and HCT116 cells (Supplementary Figure 2), while miR-18a*, the complimentary strand of miR-18a, did not increase the level of apoptosis after its transfection into SW620 cells (Supplementary Figure 3). To examine the relationship between cell viability and miR-18a expression, the MTT assay was performed in SW620 and HCT116 cells with up- or downregulated expression of miR-18a. The MTT assay showed that, while there were no changes in the cell density between the miR-18a overexpressing cells and the control cells within 48 h, the cell density was significantly decreased in the miR-18a-overexpressing cells in comparison to the levels observed in the control 72 and 96 h after transfection into SW620 cells. Conversely, in miR-18a-knockdown cells, the cell viability was not changed in comparison to that of the control at any of the time points in SW620 cells (Figure 1a, (Supplementary Figure 4). The cell viability was significantly decreased in miR-18a-overexpressing HCT116 cells and significantly increased in miR-18a-knockdown HCT116 cells (Figure 1b).

To assess the *in vivo* impact of the miR, a suspension of 1×10^6 SW620 cells was injected into the backs of nude mice to generate a xenograft model in order to confirm the suppressive effects of miR-18a overexpression on colon cancer progression. Double-stranded miR-18a or control RNA inserted in a Sendai virus envelope was injected every day into the tumors beginning the day after implantation of the cells, and the tumor sizes were measured. Figure 1c shows that the increase in the size of the tumors in the miR-18a-injected group was almost completely suppressed (1.1-fold), while the tumors in the control group increased in size by 1.6-fold. Moreover, SW620 cells that stably overexpressed miR-18a or a control vector were injected into nude mice using the same methods. The tumor size increased rapidly in the mice injected with SW620 cells treated with the control vector, but not in the cells stably overexpressing miR-18a (Figure 1d).

Immunocytochemical staining showed the Ki-67 expression to not be significantly different between the miR-18a-overexpressing cells and control cells (Supplementary Figure 5). TUNEL staining showed that there was a significant increase in the number of TUNEL-positive miR-18a overexpressing cells compared to the control and miR-18a knockdown cells (Figure 1e).

A western blotting analysis also showed that the expression levels of cleaved caspases −3, −9 and PARP were significantly increased in the miR-18a-overexpressing cells in comparison to the level observed in the control cells (Figure 1f). The cell population in each phase of the cell cycle was examined using flow cytometry. A telomere length assay revealed that the telomere length was shorter in the miR-18a-overexpressing cells than in the control cells (Supplementary Figure 6). Therefore, the overexpression of miR-18a inhibited colon cancer progression by inducing the apoptosis of the cancer cells.

miR-18a induces cancer cell apoptosis by suppressing hnRNP A1

It has been hypothesized that miR-18a targets oncogenic proteins, particularly members of the hnRNP family, a group of RNA-binding proteins.[24] hnRNP A1 possesses binding sites for miR-18a;[25,26] therefore, hnRNP A1 was the focus of the subsequent experiments. Real-time PCR showed that the mRNA for hnRNP A1 is highly expressed in colon cancer tissues and cell lines[27] (Supplementary Figures 7A–C). To determine whether the effects of miR-18a on the suppression of cancer cell progression were dependent on the expression of hnRNP A1, SW620 cells were transfected with miR-18a with or without hnRNP A1 siRNA. Targeting hnRNP A1 with siRNA inhibited cancer cell progression. Notably, the inhibitory effect induced by miR-18a was repressed in the cells transfected with the hnRNP A1 siRNA (Figure 2a). A competitor RNA with a complimentary sequence to the binding site of miR-18a to hnRNP A1 negated the cancer cell apoptosis induced by the overexpression of miR-18a (Figure 2b).

It is known that hnRNP A1 stabilizes the mRNAs of cyclin D1 and CTGF, while increasing the expression levels of these molecules, which are associated with the evasion of apoptosis.[28,29] The expression levels of cyclin D1 and CTGF were therefore examined to determine whether the overexpression of miR-18a inhibits the function of hnRNP A1. Figure 2c shows that the cyclin D1 and CTGF expression levels were significantly decreased in the SW620 cells overexpressing miR-18a. The competitor RNA repressed the downregulation of cyclin D1 and CTGF (Figures 2d and e). Conversely, the overexpression of miR-18a did not change the translation of the mRNAs encoding cell growth- and apoptosis-associated molecules, which were selected based on previous reports and were estimated targets of mRNAs in an analysis of microRNA sequences using a software program (**Targetscan, http://www.targetscan.org/vert_50/**)(Supplementary Figure 8). These findings indicate that the miR-18a-induced apoptosis of cancer cells is mediated by the creation of a complex between miR-18a and hnRNP A1.

miR-18a binds to hnRNP A1 in the cytoplasm of colon cancer cells

A binding assay demonstrated the ratio of miR-18a bound to hnRNP A1 in cell lines, including HEK 293, Caco2/bbe, HT29, HCT116, SKCO-1, SW480 and -620 cells. The HEK 293 cells were selected as non-cancer cells. The ratio of binding between miR-18a and hnRNP A1 varied in these cell lines. Approximately 8% and 30% of all miR-18a were bound to hnRNP A1 in the SW620 and HCT116 cells, respectively, while 58% of the endogenous miR-18a was bound to hnRNP A1 in the HEK cells. The binding between miR-18a and hnRNP A1 was increased 5.5-fold and 7-fold in the miR-18a-overexpressing SW620 and HCT116 cells, respectively (Figure 3a).

FITC-labeled miR-18a was transfected into the SW620 cells to assess the interaction between this protein and hnRPN A1. A western blotting analysis with immunoprecipitation and a binding assay showed that FITC-labeled miR-18a bound to hnRNP A1 was detected primarily in the cytoplasm of the SW620 cells (Figures 3b and c and Supplementary Figure 9). These findings suggest that miR-18a directly binds to hnRNP A1 in the cytoplasm of colon cancer cells.

miR-18a induces the degradation of hnRNP A1

The hnRNP A1 expression was assessed by a western blotting analysis at 3, 6, 24, 48, 72 and 96 h after transfection with miR-18a to determine whether the hnRNP A1 expression was changed by the binding to miR-18a. The hnRNP A1 expression was significantly decreased at 72 and 96 h after miR-18a transfection, while no changes in the hnRNP A1 expression were observed within 48 h (Figure 4a). Notably, the decreased expression of the hnRNP A1 protein induced by the overexpression of miR-18a was repressed by treatment with the competitor of miR-18a at 72 h, suggesting that the decreased expression of hnRNP A1 is mediated by the creation of a complex between miR18a and hnRNP A1 (Figure 4b). The mRNA level of hnRNP A1 was not decreased at 3, 8, 24, 48, 72 or 96 h (Figure 4c). Similarly, a xenograft model demonstrated that the expression of hnRNP A1 proteins, but not mRNA, was significantly lower in the tumors

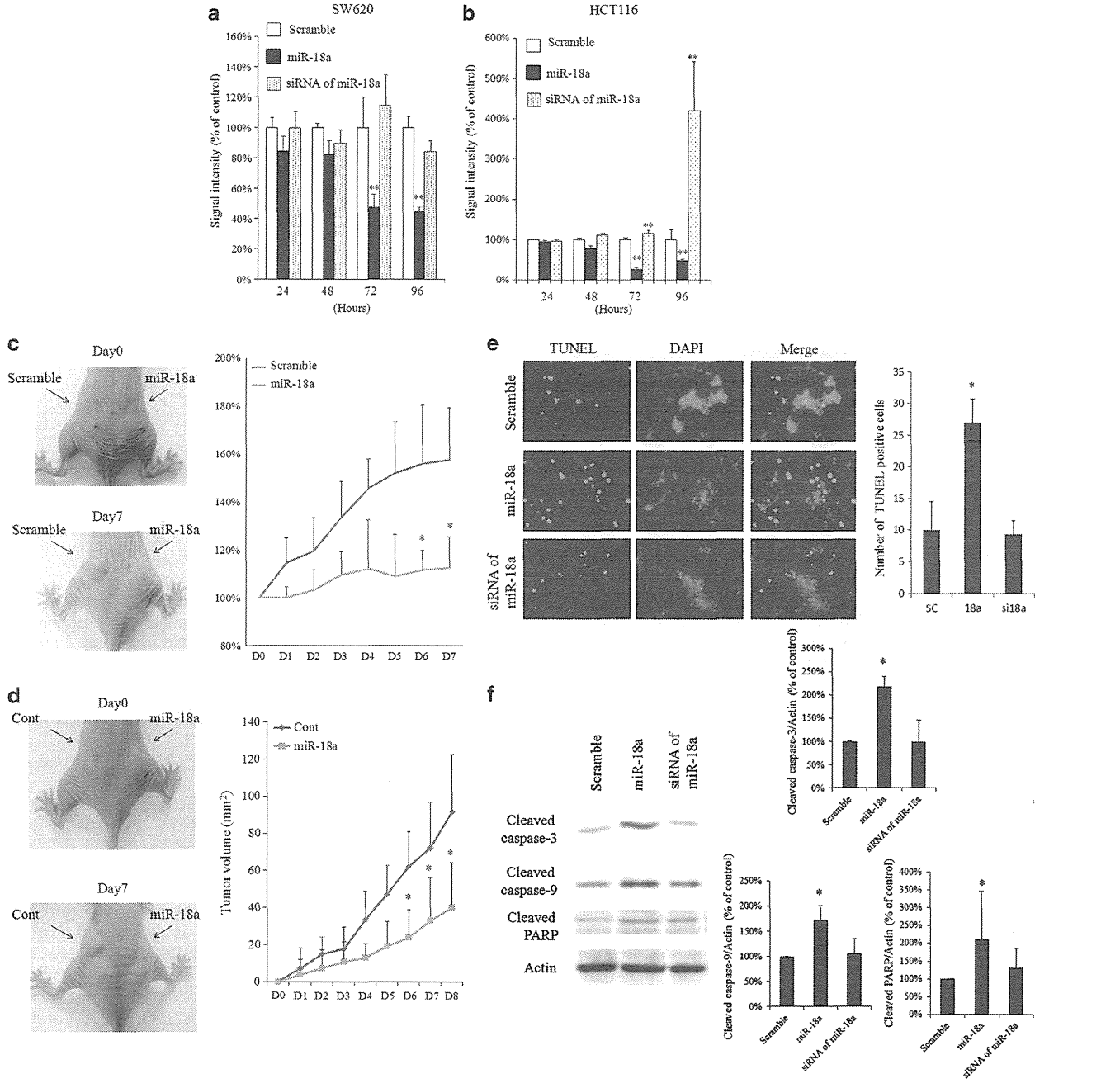

Figure 1. The overexpression of miR-18a induces the apoptosis of colon cancer cells. An MTT assay revealed that the number of live SW620 cells was significantly lower in the miR-18a overexpression group than in the control group at 72 and 96 h after transfection ($n = 5$) (**a**). An MTT assay showed that the viability of HCT116 cells was significantly lower in the miR-18a overexpression group and higher in the miR-18a siRNA-treated group than in the control group at 72 and 96 h after transfection ($n = 5$) (**b**). The xenograft model showed that the enlargement of the tumors in the miR-18a-injected group was almost completely suppressed (1.1-fold), while the tumors in the control group were enlarged as much as 1.6-fold ($n = 6$) (**c**). miR-18a stably-overexpressing and control SW620 cells were used to generate another xenograft model. The model showed that the tumor size was significantly smaller in the xenografts from SW620 cells stably overexpressing miR-18a than in the tumors generated from control cells (**d**). TUNEL staining showed the level of apoptosis to increase in the SW620 cells transfected with miR-18a in comparison to that in the cells transfected with scramble RNA (**e**). A western blotting showed analysis that the cleaved caspase-3, -9 and PARP expression levels were significantly higher in the SW620 cells transfected with double-stranded miR-18a ($n = 3$) (**f**). $^{*}P < 0.05$, $^{**}P < 0.01$.

injected with double-stranded miR-18a than in those injected with control RNA (Figure 4d). Therefore, miR-18a post-transcriptionally decreases the protein expression of hnRNP A1 by binding to hnRNP A1.

Next, the degradation rate of hnRNP A1 was assessed using single and double isotope studies to determine whether miR-18a induces its degradation. A single isotope study showed that the ^{3}H activity was significantly lower in SW620 cells transfected with double-stranded miR-18a than in control cells at 72 to 96 h after transfection (Supplementary Figure 10). An *in vivo* double isotope study confirmed that the $^{3}H/^{14}C$ ratio was significantly lower in mice transfected with double-stranded miR-18a than in those

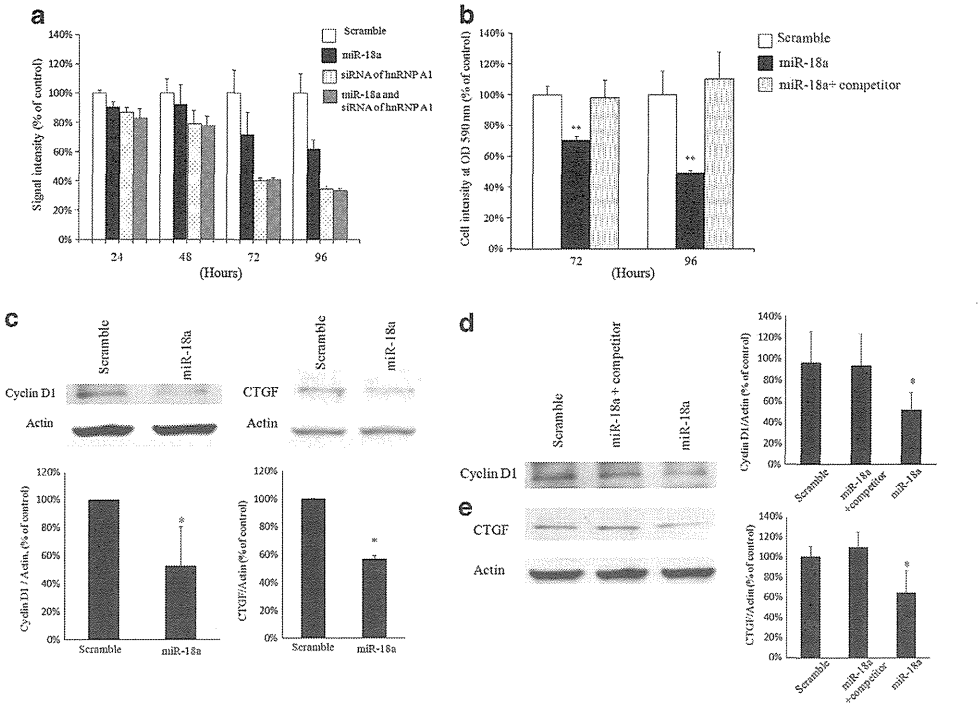

Figure 2. miR-18a induces cancer cell apoptosis by binding to hnRNP A1 and suppressing its functions. A MTT assay revealed that the overexpression of miR-18a inhibited cancer cell progression, and a siRNA targeting hnRNP A1 also inhibited cancer cell progression. The inhibitory effect of miR-18a on cancer cell progression was negated in the cells transfected with the hnRNP A1 siRNA ($n=5$) (**a**). A competitor RNA with a complimentary sequence to the binding site of miR-18a to hnRNP A1 repressed the apoptosis induced by the overexpression of miR-18a (**b**). The expression levels of cyclin D1 ($n=4$) and CTGF ($n=3$), which were upregulated by hnRNP A1, were significantly decreased in SW620 cells overexpressing miR-18a. The upper figure shows western blots and the lower one shows the results of the densitometry analysis (**c**). The competitor RNA negated the downregulation of cyclin D1 ($n=4$) (**d**) and CTGF ($n=4$) induced by the overexpression of miR-18a (**e**). $^{*}P<0.05$, $^{**}P<0.01$.

injected with control cells, suggesting that miR-18a induces the degradation of the hnRNP A1 protein (Figure 4e).

The degradation of hnRNP A1 by miR-18a is mediated by autophagy

The ubiquitination of hnRNP A1 bound to miR-18a was evaluated using a Western blotting analysis to examine the mechanisms underlying the degradation of hnRNP A1 by miR-18a. The ubiquitinated hnRNP A1 band was significantly increased in the miR-18a-overexpressing cells at 72 and 96 h in comparison with that observed in the control cells, while no changes were observed in the higher molecular bands in any group (Figure 5a). This suggests that the ubiquitination of hnRNP A1 is augmented by miR-18a overexpression, and that this leads to the subsequent proteasomal or lysosomal degradation of the protein. We then confirmed that 3-methyladenine, an inhibitor of autophagy, negated the effects of miR-18a overexpression on the hnRNP A1 expression (Figure 5b). In contrast, MG132, an inhibitor of the proteasome, did not affect the expression of hnRNP A1 (Supplementary Figure 11).

An immunocytochemical study demonstrated the coexpression of hnRNP A1 and LC3-II, a component of autophagosomes (Figure 5c). A western blotting analysis with immunoprecipitation showed that FITC-labeled miR-18a formed a complex with LC3-II and hnRNP A1 (Figure 5d). A siRNA targeting ATG7, which is also a mediator of the creation of autophagosomes, repressed the downregulation of hnRNP A1 induced by miR-18a (Figure 5e). Treatment of cells with siRNAs against both p62, a well-known molecule that selectively brings ubiquitinated proteins to autophagosomes,[30] and BAG3, which is required to process autophagolysosomal degradation,[31] also negated the decrease in the hnRNP A1 expression induced by miR-18a (Figure 5f, Supplementary Figure 12).

To examine whether normal cells possess a mechanism leading to the autophagosomal degradation of hnRNP A1 via binding with miR-18a, we performed a binding assay and a Western blotting analysis in HEK293 cells. The binding assay showed that 58% of the endogenous miR-18a bound to hnRNP A1 (Figure 3a). The western blotting analysis showed that miR-18a downregulates hnRNP A1, and this function of miR-18a is diminished by the knockdown of autophagy-related genes, such as ATG7 and p62, in HEK293 cells (Supplementary Figure 13). These results indicate that miR-18a-bound hnRNP A1 is selectively degraded by the autophagosomal pathway in cancer cells, as well as in normal cells.

DISCUSSION

The present study demonstrated that miR-18a inhibits colon cancer progression through the induction of cancer cell apoptosis. The antitumor effect of miR-18a was repressed by the treatment of cells with a competitor for the miR-18a-hnRNP A1 interaction and by the inhibition of the autophagolysosomal pathway with a specific inhibitor or with siRNAs targeting ATG7, p62 and BAG3, thus indicating that the effect of miR-18a is due to its interaction with oncogenic hnRNP A1, and the subsequent induction of the autophagolysosomal degradation of the protein. These data suggest that miRs can exert inhibitory effects on cancer progression by inducing the degradation of oncogenic proteins (Figure 6).

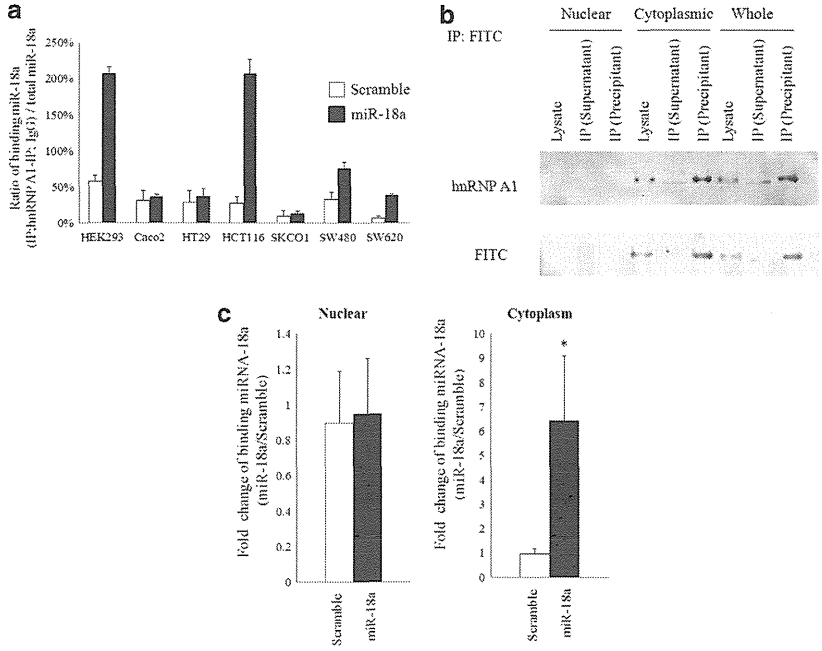

Figure 3. miR-18a binds to hnRNP A1 in the cytoplasm of colon cancer cells. The cells and tissues were lysed and immunoprecipitated using IgG and hnRNP A1 antibodies. RNA was extracted and the miR-18a expression was measured using real-time PCR (a binding assay). The assay showed that the ratio of binding between miR-18a and hnRNP A1 varied by cell line. Approximately 8% and 30% of miR-18a molecules were bound to hnRNP A1 in the SW620 and HCT116 cells, respectively, while 58% of miR-18a was bound to hnRNP A1 in HEK 293 cells (**a**). The proteins in the nucleus and cytoplasm of SW620 cells transfected with FITC-labeled miR-18a were separately extracted and immunoprecipitated with anti-FITC antibodies. The expression of hnRNP A1 was examined by a western blot analysis. The upper blot was detected by a western blot analysis with immunoprecipitation by anti-hnRNP antibodies. The lower blot was detected with immunoprecipitation by anti-FITC antibodies. The hnRNP A1 bound to miR-18a was primarily expressed in the cytoplasm of SW620 cells (**b**). A binding assay showed that the FITC-labeled miR-18a bound to hnRNP A1 was primarily detected in the cytoplasm of SW620 cells (**c**). ($n=3$) $^*P<0.05$.

miRs generally function by controlling the translation of mRNAs in cancer cells. For example, let-7a inhibits the translation of MYC mRNA in lymphoma cells.[19] miR-107, -22, -143, -34a and -21 target the mRNAs of HIF-1,[32] p21,[33] metastasis-associated in colon cancer-1,[34] fos-related antigen 1,[35] and transforming growth factor beta receptor 2[36] in colon cancer cells, respectively. The mRNA of estrogen receptors is targeted by miR-18a in hepatocellular carcinoma cells,[20] breast cancer cells[21] and dicers in bladder cancer cells;[22] however, the target of miR-18a in colon cancer had not been identified, although miR-18a is highly expressed in colon cancer cells.[23] Recently, Eiring *et al.*[24] proposed the possibility that miRs directly bind to target proteins and inhibit the protein functions and concluded that miRs can target not only mRNAs but also proteins. However, the role of binding between miRs and hnRNPs in cancer progression and the fate of the miR-hnRNP A1 complex have not yet been clarified. The present study demonstrated, for the first time, that the binding between miR-18a and hnRNP A1 is a trigger for the ubiquitination and degradation of oncogenic hnRNP A1 via the autophagolysosomal pathway. Therefore, the overexpression of miR-18a is thought to continuously, not temporally, inhibit the oncogenic function of hnRNP A1. No therapeutic strategies for treating colon cancers by targeting hnRNPs have thus far been established. However, miR-18a transfection is a feasible option for treating colon cancers, and possibly other types of cancers in which hnRNP A1 is upregulated.

The present study showed that transfected miR-18a is bound to hnRNP A1 in the cytoplasm of colon cancer cells. Most hnRNP A1 is expressed in the nucleus in normal epithelia, binds to pri-miR-18a and contributes to the maturation of miR-18a.[25] Mature miR-18a is then transported from the nucleus to the cytoplasm, where it controls the translation of mRNAs. The present study suggests that when the hnRNP A1 expression is increased in normal cells, the maturation of miR-18a is promoted in the nucleus, and the increased mature miR-18a is thereafter transported to the cytoplasm, where it degrades the overexpressed hnRNP A1. This appears to be a feedback system between miRs and hnRNPs. Conversely, this feedback system is thought to be impaired in cancer cells because hnRNPs, including hnRNP A1, -I and K, are highly expressed in the cytoplasm of colon cancer cells, particularly in metastatic lymph nodes. The excess expression of cytoplasmic hnRNPs appears to promote with the malignant behavior of colon cancer.[37] Accordingly, mature miR-18a is thought to create a complex with excessively-expressed hnRNP A1 in the cytoplasm and inhibits its function by inducing autophagolysosomal degradation. The present study also showed that, while the expression levels of both miR-18a and hnRNP A1 are increased in colon cancer cells, the transfection of mature miR-18a still inhibits cancer progression by inducing apoptosis both *in vitro* and *in vivo*. Our binding assay showed that, in colon cancer cells (SW620 cells), only 8% of the miR-18a molecules are bound to hnRNP A1, whereas 58% of endogenous miR-18a in HEK 293 cells was present in a complex with hnRNP A1, suggesting that a large amount of free hnRNP A1 is present in the cytoplasm and exerts its oncogenic functions in cancer cells by binding to target mRNAs. Transfection of miR-18a increased the miR-18a-hnRNP A1 complex 6-fold, thereby inhibiting the oncogenic functions of hnRNP A1.

The present study proposes that miR-18a induces the degradation of hnRNP A1 through the autophagolysosomal pathway. It has recently been shown that miR-18a upregulated the autophagy and gene expression of ataxia telangiectasia mutated, which

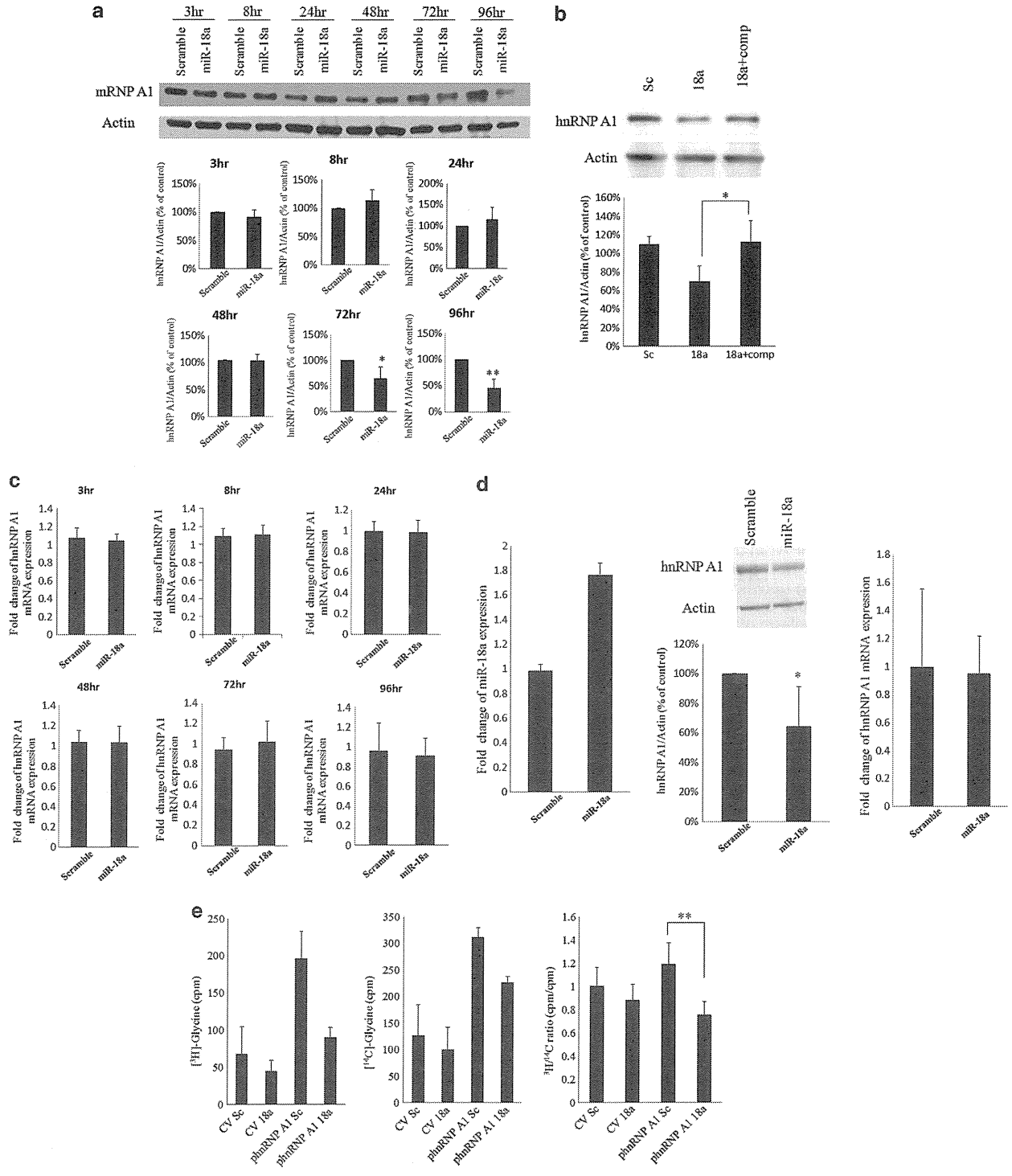

Figure 4. miR-18a induces the degradation of hnRNP A1. The expression of hnRNP A1 was assessed by a western blotting analysis at 24, 48, 72 and 96 h after transfection of the cells with miR-18a. The hnRNP A1 expression was significantly decreased at 72 and 96 h after miR-18a transfection ($n = 3$) (**a**). The decreased expression of hnRNP A1 proteins induced by the overexpression of miR-18a was negated by treatment with the competitor of miR-18a ($n = 3$) (**b**). The hnRNP A1 mRNA level did not decrease at 3, 8, 24, 48, 72 or 96 h after transfection with miR-18a ($n = 3$) (**c**). A xenograft model showed that the expression of miR-18a was increased (left) and the expression of hnRNP A1 protein was decreased (center) in the tumors injected with double-stranded miR-18a, in comparison to that observed in the tumors injected with control RNA, while the hnRNP A1 mRNA level was not significantly different in these groups (right) ($n = 3$) (**d**). The mice were injected with 100 μCi of [^{3}H]-glycine 3 h after transfection of the expression vector for hnRNP A1 and/or double-stranded miR-18a. The mice were again injected with an expression vector for hnRNP A1 72 h later. The mice were injected with 12.5 μCi of [14C]-glycine 3 h later and then were killed after an additional 3 h. Protein samples obtained from the intestines were immunoprecipitated with hnRNP A1 antibodies, and the radioactivity was measured (a double isotope study). This assay showed that the ^{3}H/^{14}C ratio was significantly lower in the mice transfected with double-stranded miR-18a than in those injected with the control cells ($n = 3$) (**e**). $^*P < 0.05$, $^{**}P < 0.01$.

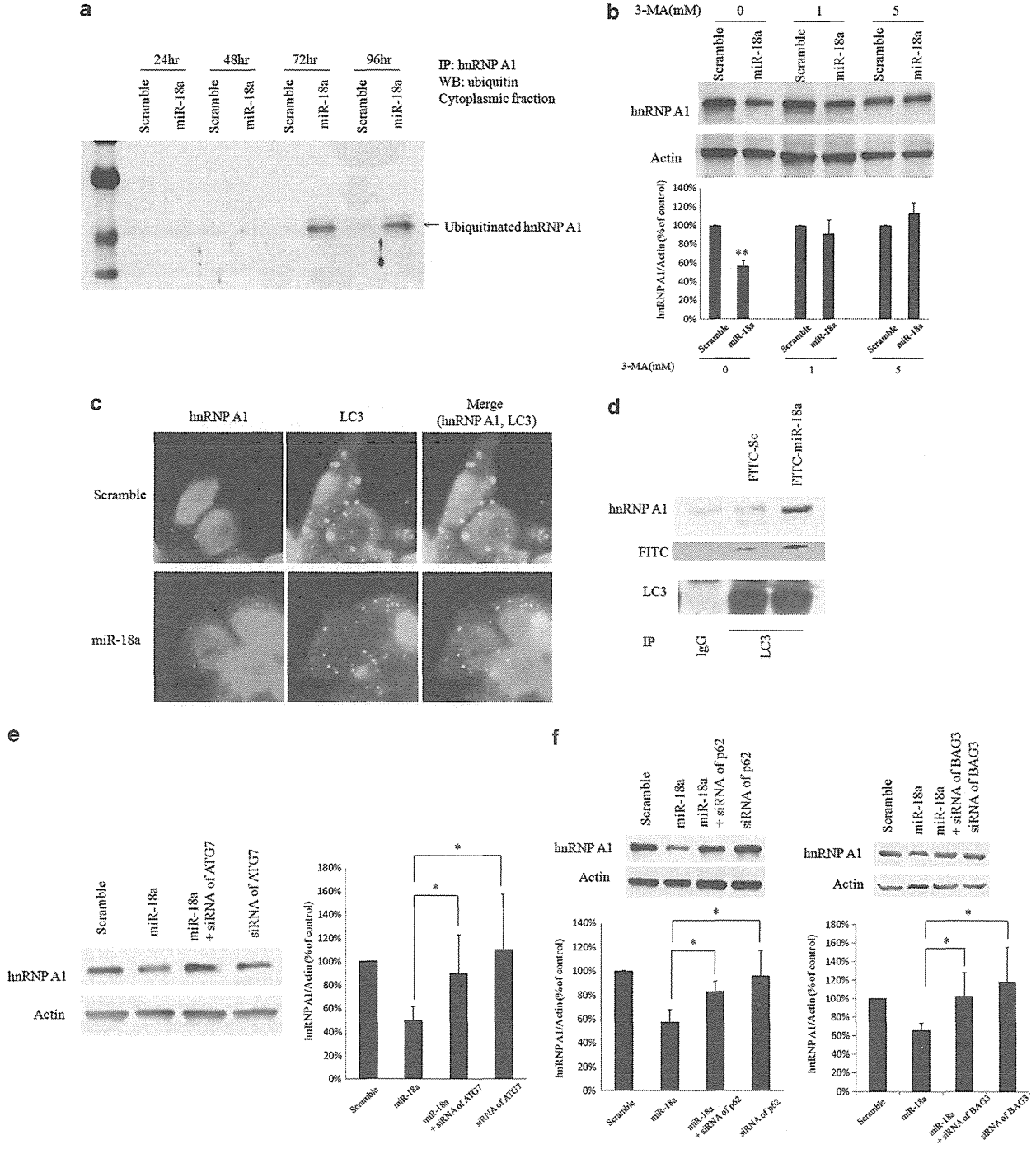

Figure 5. Autophagy mediates the degradation of hnRNP A1 by miR-18a in colon cancer cells. A western blotting analysis revealed that ubiquitinated hnRNP A1 band was significantly increased in miR-18a-overexpressing cells in comparison to that observed in the control cells at 72 and 96 h, while there were no significant differences in the intensities of the higher molecular bands between the groups ($n=3$) (**a**). 3-methyladenine, an inhibitor of autophagy, repressed the inhibitory effects of miR-18a overexpression on the expression of hnRNP A1 ($n=3$) (**b**). Immunocytochemistry demonstrated the coexpression of hnRNP A1 and LC3-II, a component of autophagosomes ($n=3$) (**c**). A western blotting analysis using immunoprecipitation with anti-FITC antibodies in SW620 cells transfected with FITC-labeled miR-18a showed that miR-18a formed a complex with hnRNP A1 and LC3-II, an essential component of the autophagy process ($n=6$) (**d**). Treatment with a siRNA targeting ATG7, an essential mediator of the creation of autophagosomes, repressed the effects of miR-18a on the downregulation of hnRNP A1 ($n=3$) (**e**). The treatment with a siRNA targeting p62, which selectively brings ubiquitinated proteins to autophagosomes, also repressed the decrease in the hnRNP A1 expression induced by miR-18a ($n=3$) (left). This also occurred following treatment with a siRNA targeting BAG3, which is required for the process of autophagolysosomal degradation ($n=3$) (right) (**f**). $^{*}P<0.05$, $^{**}P<0.01$.

enhanced the autophagy process.[38] Taken together, these findings suggest that miR-18a induces the degradation of oncogenic hnRNP A1 by forming a complex with the protein, as well as by enhancing the autophagy pathway itself. miR-18a is therefore considered to be a multifunctional molecule which regulates both gene expression and protein degradation.

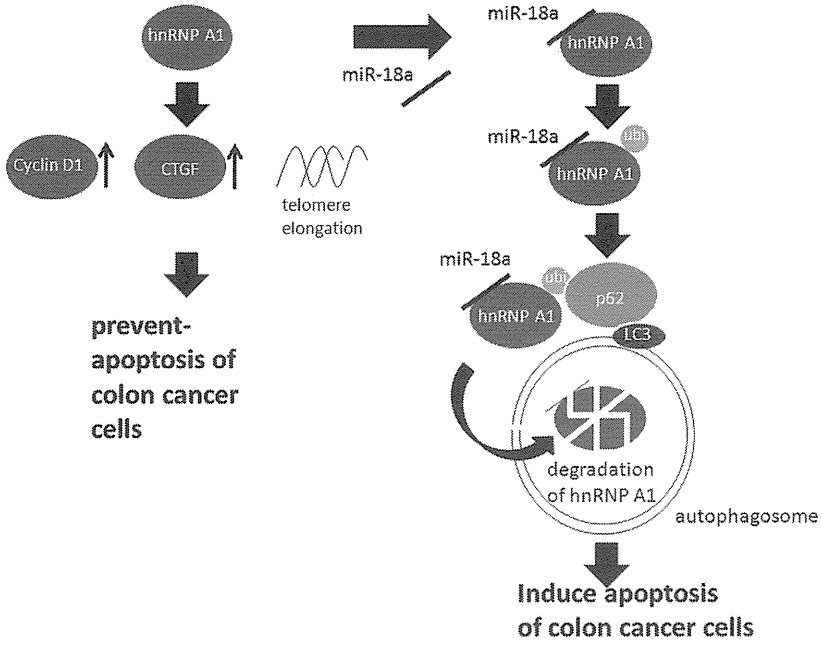

Figure 6. A scheme of the miR-18a-mediated pathway that induces the apoptosis of colon cancer cells. miR-18a inhibits colon cancer progression by inducing cancer cell apoptosis by binding to oncogenic hnRNP A1 and inducing the autophagolysosomal degradation of the protein.

In summary, the current study proposed a novel function of miR-18a in the inhibition of colon cancer progression via the binding and downregulation of oncogenic hnRNP A1 in the cytoplasm. This function is considered to be reproducible for other miRs, thus providing new insights into the eventual development of new therapeutic strategies to treat various malignancies in which hnRNPs are associated with tumor progression.

MATERIALS AND METHODS

Human intestinal epithelia

Biopsy specimens of normal mucosa were obtained from the colons of patients with colon cancer during colonoscopy. Written informed consent was obtained from all patients, and the ethics committee of Asahikawa Medical University gave its approval for this study.

Cell culture

Human colon cancer cell lines, Caco2/bbe, HT-29, SKCO-1, SW480 and SW620, were purchased from the ATCC and grown in high-glucose Dulbecco's Modified Eagle's Medium (Caco2/bbe, HT-29, SKCO1) or Roswell Park Memorial Institute 1640 (SW480 and SW620) supplemented with 10% (vol/vol) fetal bovine serum, 2 mM of L-glutamine, 50 U/ml of penicillin, 50 μg/ml of streptomycin and 10 μg/ml of transferrin (all purchased from Invitrogen/GIBCO, Grand Island, NY, USA) in a humidified atmosphere of 5% CO_2. The cells were plated on 6- or 12-well plates at a density of 10^5 cells/cm^2.

Protein extraction

The total proteins were extracted from samples using a Mammalian Cell Extraction Kit (BioVision, Mountain View, CA, USA). The cells were lysed for immunoprecipitation using Buffer A (10 mM of Tris-Cl, pH 7.9, 60 mM of KCl, 1 mM of EDTA and 1 mM of dithiothreitol) containing 0.1% Nonidet P-40, 1 mM of phenylmethylsulfonyl fluoride and a complete protease inhibitor (Roche Molecular Biochemicals, Indianapolis, IN, USA). To obtain proteins from the cytosolic organelles, the cells were lysed in gradient buffer (0.25 M sucrose, 20 mM of HEPES (pH 7.0), 0.02% sodium azide and a complete protease inhibitor) and then homogenized using a needle. The cell suspensions were centrifuged for 5 min at 1200 r.p.m., and the supernatants were harvested as cytosolic organelle samples. The cells were lysed using cytosol lysis buffer (10 mM of HEPES-KOH (pH 7.8), 10 mM of KCl, 0.1 mM of EDTA, RNase inhibitor (Applied Biosystems, Foster City, CA, USA, 40 units/ml) and complete protease cocktail) and nucleus lysis buffer (50 mM HEPES-KOH (pH 7.8), 420 mM of KCl, 0.1 mM of EDTA, 5 mM of $MgCl_2$, 20% Glycerol, RNase inhibitor (40 units/ml) and complete protease cocktail) in order to separately extract the proteins from the cytosol and nucleus. The cells were washed with PBS and lysed in cytosol lysis buffer before being subjected to five minutes of incubation, followed by five minutes of centrifugation at 1200 r.p.m., and the supernatants were harvested. The pellets were then resuspended in cytosol lysis buffer and centrifuged again. Finally, the pellets were gently resuspended in nuclear lysis buffer and used as the nucleoplasmic fraction.

Inhibitors

MG132 (ENZO Life Science Inc., Farmingdale, NY, USA) or 3-Methiladenine (R&D systems, Minneapolis, MN, USA) was used to inhibit the proteasomal or autophagosomal degradation of proteins, respectively.

Plasmids, RNAs and transfections

cDNA was obtained using reverse transcription (RT)-PCR of SW620 cells with a high-capacity cDNA reverse transcription kit (Applied Biosystems). hnRNP A1 DNA was amplified using PCR with a primer set in which the 5′ end of the upstream region contained the *Nhe*I restriction site, and the downstream region contained the *Bam HI* restriction site (sense, 5′-agtcagctagccttcaccctgccgtcatg-3′, anti-sense, 5′-agtcaggatcccctgctaag ctttgtttcc-3′). The *Nhe*I/*Bam HI* digested PCR product was cloned into the multicloning site of the pIRES puro2 vector (CLONTECH Laboratories, Inc., Mountain View, CA, USA). RNAs were synthesized by Hokkaido System Science Co., Ltd. The nucleotide sequences of the miR-18a duplex were: sense, 5′-uaaggugcaucuagugcagaua-3′ and antisense, 5′-acugcccuaagug-cuccuucu-3′. A negative control with a scrambled miRNA sequence was prepared by annealing two synthetic RNAs: sense, 5′-uacguacuaucgcgcg-gau-3′ and antisense, 5′-auccgcgcgauaguacgua-3′. siRNAs for hnRNP A1 and BAG3 and siRNAs for ATG7 and SQSTM1/p62 were purchased from Santa Cruz Biotechnology (Santa Cruz, CA, USA) and Cell Signaling Technology, Inc. (Danvers, MA, USA) respectively. The cells were seeded 24 h prior to transfection, and transfection was performed using the HVJ Envelope VECTOR KIT (Ishihara Sangyo, Osaka, Japan).

Lentiviruses and infections

The lentivirus containing the whole sequence of the target microRNA (control and miR-18a) was purchased from Applied Biological Materials,

Inc. (Richmond, BC, Canada) Cells were grown in culture media containing polybrane (Santa Cruz Biotechnology) with the lentivirus vector and were selected in media containing 5 μg/ml puromycin. Cells with the lentivirus vector containing the whole sequence of the target microRNA were used for the xenograft model.

Immunoprecipitation

Each lysate sample was immunoprecipitated using IgG, hnRNP A1 or FITC antibodies (1 μg each), then 30 μl of protein G Sepharose 4 Fast Flow (GE Healthcare, Buckinghamshire, UK) was added. The mixtures were incubated overnight at 4°C, washed three times with PBS and boiled in Laemmli buffer to extract the proteins.

Western blot analyses

Equal amounts of protein were resolved using SDS–PAGE (12.5%), blotted onto a nitrocellulose membrane and then blocked in PBS with 0.05% (vol/vol) Tween 20 (T-PBS) containing 1% (wt/vol) bovine serum albumin. The blot was incubated overnight at 4°C with primary antibodies. The monoclonal antibodies against hnRNP A1 (Novus Biologicals, Littleton, CO, USA), RUNX 1 (Novus Biologicals), FITC (Novus Biologicals), ATG7 (Cell Signaling Technology), cyclin D1 (Santa Cruz Biotechnology), cyclin D2 (Abcam, Tokyo, Japan), NEDD9 (Abcam), estrogen receptor α (Abcam) and CD166 (Abcam), and the polyclonal antibodies against SQSTM1/p62 (Novus Biologicals), IGF1 (Abcam), BAG3 (Abnova), LC-3 (Medical & Biological Laboratories co., Ltd, Nagoya, Japan) and PTP4A3 (Abcam) were used as primary antibodies. The blots were then washed in T-PBS, incubated with a HRP-conjugated secondary antibody (R&D Systems), washed in T-PBS and then developed using either the Super-Signal West Pico or the femto enhanced chemiluminescence system (Thermo science, Waltham, MA, USA). The average protein expression was normalized to the actin expression (BD transduction laboratories, Lexington, KY, USA).

Real-time PCR

Total RNA was extracted using an RNeasy mini kit (Qiagen, Tokyo, Japan) according to the manufacturer's instructions. The mRNAs were reverse transcribed using a high-capacity cDNA reverse transcription kit (Applied Biosystems). The gene expression was measured using specific primers (hnRNP A1: sense, 5′-tcgtcagcttgctccttttctg-3′, anti-sense, 5′-atgacggcag ggtgaagaga-3′, taqman probe, 5′-ccgccgaagaagcatcgttaaagt-3′; CTGF: sense, 5′-tgtgtgacgagcccaagga-3′, anti-sense, 5′-tctgggccaaacgtgtcttc-3′, taqman probe, 5′-tggttgggcctgccctcgc-3′) in triplicate. The average mRNA expression was normalized to the 18S rRNA expression (Applied Biosystems).

Binding assay

The cells were lysed using lysis buffer A (10 mM of Tris-Cl, pH 7.9, 60 mM of KCl, 1 mM of EDTA and 1 mM of dithiothreitol) containing 0.1% Nonidet P-40, 1 mM of phenylmethylsulfonyl fluoride and complete protease inhibitors. The lysates were clarified by centrifugation for 10 min at 12 000 r.p.m., and an RNase inhibitor (40 units/ml) was added. The cell lysates were immunoprecipitated using IgG or hnRNP A1 antibodies (1 μg each) and 30 μl of protein G Sepharose 4 Fast Flow. RNA was extracted from the beads using phenol-chloroform extraction and was reverse-transcribed using a taqman microRNA reverse transcription kit (Applied Biosystems). The resulting cDNA was measured using real-time PCR for hsa-miR-18a (Applied Biosystems).

Immunocytochemistry

The cells were plated on chamber slides, which were fixed in 4% paraformaldehyde, washed extensively with PBS, permeabilized with 0.1% Triton X-100 and blocked in 3% BSA in PBS. The slides were then sequentially incubated with primary antibodies, washed with PBS and incubated with Alexa 488 and/or 594-conjugated secondary antibodies (Invitrogen-Molecular Probes, Carlsbad, CA, USA). The nuclei were counterstained with DAPI (Lonza, Tokyo, Japan). The cells were mounted with an anti-fade mounting medium, and the immunofluorescence was visualized using a fluorescence microscope (KEYENCE corporation, Osaka, Japan).

Telomere length assay

The cells were washed with PBS and incubated with lysis buffer (25 mM of Tris-HCl (pH 8.0), 50 mM of EDTA (pH 8.0) 1% SDS) 400 μl/sample, 10 mg/ml of protein kinase K 10 μl/sample) at 55°C overnight. DNA was extracted using phenol-chloroform extraction and was dissolved in distilled water. The telomere length was detected using a TeloTTAGGG telomere length assay (Roche Applied Science, Penzberg, Germany) according to the manufacturer's instructions.

MTT assay

The cells were seeded on 96-well microplates at 1.0×10^4 per well 24 h prior to transfection. The cell growth was assessed using an MTT cell proliferation kit according to the manufacturer's instructions (Roche Applied Science). The optical density was measured at a 590 nm test wavelength and a 620 nm reference wavelength.

Radioactive materials

The [^{3}H]-glycine and [^{14}C]-glycine were purchased from PerkinElmer, Japan.

Isotope studies

Each group of cells in the single isotope study was treated with [^{3}H]-glycine for 24 h. Next, the complex of expression vectors of hnRNP A1 and double-stranded miR-18a enclosed using the HVJ Envelope VECTOR KIT was added to the cells. In the other set of experiments, each group of mice in the double isotope study received vectors encoding hnRNP A1 and double-stranded miR-18a and were injected with 100 μCi of [^{3}H]-glycine 3 h later. Each group was given a booster injection of an expression vector for hnRNP A1 again after an additional 72 h. Thereafter, the mice were injected with 12.5 μCi of [14C]-glycine 3 h later, and then killed 3 h after that. Protein samples were collected from the intestines using lysis buffer A and were analyzed by immunoprecipitation with hnRNP A1 antibodies. The radioactivity was measured in a Beckman scintillation spectrometer.

Xenografts

The protocols for the animal experiments were approved by the Asahikawa Medical University Institutional Animal Care and Use Committee. SW620 cells (1×10^6 cells) were injected into male BALB/c nude mice. Double-stranded miR-18a or control RNA was transfected daily starting one week after the injection of SW620 cells for tumor treatment.

CONFLICT OF INTEREST

The authors declare no conflicts of interest.

REFERENCES

1 Capon DJ, Seeburg PH, McGrath JP, Hayflick JS, Edman U, Levinson AD *et al.* Activation of Ki-ras2 gene in human colon and lung carcinomas by two different point mutations. *Nature* 1983; **304**: 507–513.
2 Forrester K, Almoguera C, Han K, Grizzle WE, Perucho M. Detection of high incidence of K-ras oncogenes during human colon tumorigenesis. *Nature* 1987; **327**: 298–303.
3 Guan RJ, Fu Y, Holt PR, Pardee AB. Association of K-ras mutations with p16 methylation in human colon cancer. *Gastroenterology* 1999; **116**: 1063–1071.
4 Nigro JM, Baker SJ, Preisinger AC, Jessup JM, Hostetter R, Cleary K *et al.* Mutations in the p53 gene occur in diverse human tumour types. *Nature* 1989; **342**: 705–708.
5 Powell SM, Zilz N, Beazer-Barclay Y, Bryan TM, Hamilton SR, Thibodeau SN *et al.* APC mutations occur early during colorectal tumorigenesis. *Nature* 1992; **359**: 235–237.
6 Taft RJ, Pang KC, Mercer TR, Dinger M, Mattick JS. Non-coding RNAs: regulators of disease. *J Pathol* 2010; **220**: 126–139.
7 Mattick JS, Gagen MJ. The evolution of controlled multitasked gene networks: the role of introns and other noncoding RNAs in the development of complex organisms. *Mol Biol Evol* 2001; **18**: 1611–1630.
8 Bartel DP. MicroRNAs: genomics, biogenesis, mechanism, and function. *Cell* 2004; **116**: 281–297.
9 Winter J, Jung S, Keller S, Gregory RI, Diederichs S. Many roads to maturity: microRNA biogenesis pathways and their regulation. *Nat Cell Biol* 2009; **11**: 228–234.
10 Eulalio A, Huntzinger E, Izaurralde E. Getting to the root of miRNA-mediated gene silencing. *Cell* 2008; **132**: 9–14.

11 Filipowicz W, Bhattacharyya SN, Sonenberg N. Mechanisms of post-transcriptional regulation by microRNAs: are the answers in sight? *Nat Rev Genet* 2008; **9**: 102–114.
12 Lee RC, Feinbaum RL, Ambros V. The C. elegans heterochronic gene lin-4 encodes small RNAs with antisense complementarity to lin-14. *Cell* 1993; **75**: 843–854.
13 Wienholds E, Kloosterman WP, Miska E, Alvarez-Saavedra E, Berezikov E, de Bruijn E *et al.* MicroRNA expression in zebrafish embryonic development. *Science* 2005; **309**: 310–311.
14 Wightman B, Ha I, Ruvkun G. Posttranscriptional regulation of the heterochronic gene lin-14 by lin-4 mediates temporal pattern formation in C. elegans. *Cell* 1993; **75**: 855–862.
15 Calin GA, Dumitru CD, Shimizu M, Bichi R, Zupo S, Noch E *et al.* Frequent deletions and down-regulation of micro- RNA genes miR15 and miR16 at 13q14 in chronic lymphocytic leukemia. *Proc Natl Acad Sci USA* 2002; **99**: 15524–15529.
16 He L, Thomson JM, Hemann MT, Hernando-Monge E, Mu D, Goodson S *et al.* A microRNA polycistron as a potential human oncogene. *Nature* 2005; **435**: 828–833.
17 Johnson SM, Grosshans H, Shingara J, Byrom M, Jarvis R, Cheng A *et al.* RAS is regulated by the let-7 microRNA family. *Cell* 2005; **120**: 635–647.
18 Ventura A, Young AG, Winslow MM, Lintault L, Meissner A, Erkeland SJ *et al.* Targeted deletion reveals essential and overlapping functions of the miR-17 through 92 family of miRNA clusters. *Cell* 2008; **132**: 875–886.
19 Sampson VB, Rong NH, Han J, Yang Q, Aris V, Soteropoulos P *et al.* MicroRNA let-7a down-regulates MYC and reverts MYC-induced growth in Burkitt lymphoma cells. *Cancer Res* 2007; **67**: 9762–9770.
20 Liu WH, Yeh SH, Lu CC, Yu SL, Chen HY, Lin CY *et al.* MicroRNA-18a prevents estrogen receptor-alpha expression, promoting proliferation of hepatocellular carcinoma cells. *Gastroenterology* 2009; **136**: 683–693.
21 Zhao Y, Deng C, Wang J, Xiao J, Gatalica Z, Recker RR *et al.* Let-7 family miRNAs regulate estrogen receptor alpha signaling in estrogen receptor positive breast cancer. *Breast Cancer Res Treat* 2011; **127**: 69–80.
22 Tao J, Wu D, Li P, Xu B, Lu Q, Zhang W. microRNA-18a, a member of the oncogenic miR-17-92 cluster, targets Dicer and suppresses cell proliferation in bladder cancer T24 cells. *Mol Med Rep* 2012; **5**: 167–172.
23 Motoyama K, Inoue H, Takatsuno Y, Tanaka F, Mimori K, Uetake H *et al.* Over- and under-expressed microRNAs in human colorectal cancer. *Int J Oncol* 2009; **34**: 1069–1075.
24 Eiring AM, Harb JG, Neviani P, Garton C, Oaks JJ, Spizzo R *et al.* miR-328 functions as an RNA decoy to modulate hnRNP E2 regulation of mRNA translation in leukemic blasts. *Cell* 2010; **140**: 652–665.
25 Guil S, Caceres JF. The multifunctional RNA-binding protein hnRNP A1 is required for processing of miR-18a. *Nat Struct Mol Biol* 2007; **14**: 591–596.
26 Michlewski G, Guil S, Semple CA, Caceres JF. Posttranscriptional regulation of miRNAs harboring conserved terminal loops. *Molecular cell* 2008; **32**: 383–393.
27 Ushigome M, Ubagai T, Fukuda H, Tsuchiya N, Sugimura T, Takatsuka J *et al.* Up-regulation of hnRNP A1 gene in sporadic human colorectal cancers. *Int J Oncol* 2005; **26**: 635–640.
28 Thiele BJ, Doller A, Kahne T, Pregla R, Hetzer R, Regitz-Zagrosek V. RNA-binding proteins heterogeneous nuclear ribonucleoprotein A1, E1, and K are involved in post-transcriptional control of collagen I and III synthesis. *Circ Res* 2004; **95**: 1058–1066.
29 Jo OD, Martin J, Bernath A, Masri J, Lichtenstein A, Gera J. Heterogeneous nuclear ribonucleoprotein A1 regulates cyclin D1 and c-myc internal ribosome entry site function through Akt signaling. *J Biol Chem* 2008; **283**: 23274–23287.
30 Kirkin V, McEwan DG, Novak I, Dikic I. A role for ubiquitin in selective autophagy. *Molecular cell* 2009; **34**: 259–269.
31 Kettern N, Rogon C, Limmer A, Schild H, Hohfeld J. The Hsc/Hsp70 co-chaperone network controls antigen aggregation and presentation during maturation of professional antigen presenting cells. *PLoS One* 2011; **6**: e16398.
32 Yamakuchi M, Lotterman CD, Bao C, Hruban RH, Karim B, Mendell JT *et al.* P53-induced microRNA-107 inhibits HIF-1 and tumor angiogenesis. *Proc Natl Acad Sci USA* 2010; **107**: 6334–6339.
33 Tsuchiya N, Izumiya M, Ogata-Kawata H, Okamoto K, Fujiwara Y, Nakai M *et al.* Tumor suppressor miR-22 determines p53-dependent cellular fate through post-transcriptional regulation of p21. *Cancer Res* 2011; **71**: 4628–4639.
34 Zhang Y, Wang Z, Chen M, Peng L, Wang X, Ma Q *et al.* MicroRNA-143 targets MACC1 to inhibit cell invasion and migration in colorectal cancer. *Mol Cancer* 2012; **11**: 23.
35 Wu J, Wu G, Lv L, Ren YF, Zhang XJ, Xue YF *et al.* MicroRNA-34a inhibits migration and invasion of colon cancer cells via targeting to Fra-1. *Carcinogenesis* 2012; **33**: 519–528.
36 Yu Y, Kanwar SS, Patel BB, Oh PS, Nautiyal J, Sarkar FH *et al.* MicroRNA-21 induces stemness by downregulating transforming growth factor beta receptor 2 (TGFbetaR2) in colon cancer cells. *Carcinogenesis* 2012; **33**: 68–76.
37 Hope NR, Murray GI. The expression profile of RNA-binding proteins in primary and metastatic colorectal cancer: relationship of heterogeneous nuclear ribonucleoproteins with prognosis. *Hum Pathol* 2011; **42**: 393–402.
38 Qased AB, Yi H, Liang N, Ma S, Qiao S, Liu X. MicroRNA-18a upregulates autophagy and ataxia telangiectasia mutated gene expression in HCT116 colon cancer cells. *Mol Med Report* 2013; **7**(2): 559–564.

Supplementary Information accompanies this paper on the Oncogene website (http://www.nature.com/onc)

Th1/Th17-Mediated Interstitial Pneumonia in Chronic Colitis Mice Independent of Intestinal Microbiota

Yasuhiro Nemoto,* Takanori Kanai,† Masahiro Takahara,*,‡ Shigeru Oshima,* Ryuichi Okamoto,* Kiichiro Tsuchiya,* Satoshi Matsumoto,§ and Mamoru Watanabe*

Although intestinal microbiota are essential for the development of T cell–mediated colitis, it remains undetermined whether they enhance or suppress the chronic extraintestinal inflammation that often complicates inflammatory bowel diseases. In this study, we investigate the role of intestinal microbiota in the development of colitis and extraintestinal manifestations in a mouse model in which colitis was induced in SCID mice by adoptive transfer of $CD4^+CD45RB^{high}$ T cells. Under specific pathogen-free conditions, these mice developed both colitis and extraintestinal interstitial pneumonia, whereas mice given a mixture of antibiotics did not develop colitis, but, surprisingly, developed Th1/Th17-mediated IP. Irrespective of antibiotic treatment, cotransfer of $CD4^+CD25^+$ regulatory T cells suppressed the development of pneumonitis and colitis, with all local $CD4^+CD45RB^{high}$ T cell–derived cells converted to $CD44^{high}CD62L^-IL\text{-}7R\alpha^{high}$ effector–memory T cells. Retransfer of $CD4^+$ effector–memory T cells from the lungs of antibiotic-treated mice with IP not only induced IP in both antibiotic-treated and -untreated recipients but also induced colitis in the untreated recipients. In summary, we have established a unique model of Th1/Th17-mediated IP in microbiota-free and antibiotic-treated mice. This model may be valuable in investigating the immunological mechanisms underlying extraintestinal disorders in patients with inflammatory bowel disease. *The Journal of Immunology*, **2013, 190: 6616–6625.**

Inflammatory bowel diseases (IBD) are caused by an excessive, tissue-damaging chronic inflammatory response, due largely to inappropriate activation of the immune system, with most patients having chronic disease (1, 2). The presence of commensal microbiota in the gut appears to be of crucial importance in the pathogenesis of IBD (1, 2). For example, germ-free (GF) rodent models of IBD are characterized by the absence of intestinal inflammation (3), indicating that intestinal microbiota are indispensable contributors to the pathogenesis of chronic T cell–mediated intestinal inflammation. A hallmark of T cell–mediated immune reactions to intestinal microbiota in IBD would be the continual generation of microbiota-specific colitogenic memory $CD4^+$ T cells (4). Surviving memory T cells become functionally impaired in the absence of MHC class II signals (5), providing further evidence that persistent Ags help maintain $CD4^+$ memory T cells. In addition, using a mouse model of colitis, generated by transfer of $CD4^+CD45RB^{high}$ T cells, with a reduction in regulatory T (Treg) cells, we previously reported that large numbers of $CD4^+CD44^+CD62L^-IL\text{-}7R\alpha^{high}$ effector–memory T (T_{EM}) cells proliferated in the colonic lamina propria (LP) (6). These cells reacted with intestinal bacterial Ags in vitro (7) and induced colitis when transferred to new SCID mice (8). Taken together, these findings data suggest that memory $CD4^+$ T cells reactive against intestinal bacteria are essential in the pathogenesis of chronic colitis.

IBD is often associated with extraintestinal manifestations, including conjunctivitis, uveitis, iritis, erythema nodosum, pyoderma gangrenosum, primary sclerosing cholangitis, and arthritis (9). These manifestations affect not only sites at which intestinal bacteria may be present, such as the skin and bile duct, but sites far from intestinal bacterial Ags, such as the eyes and joints. To date, it remains undetermined whether intestinal bacteria are essential for the development of extraintestinal manifestations of IBD.

Several recent studies have demonstrated that intestinal microbiota also affects the development of chronic systemic diseases, including diabetes mellitus, multiple sclerosis, and rheumatoid arthritis (10). For example, commensal gut flora are essential in triggering the activation of autoantibody-producing B cells in mice with experimental autoimmune encephalomyelitis, a model for multiple sclerosis in humans (11).

We therefore hypothesized that the intestinal microbiota modulate the development of extraintestinal manifestations in IBD. To investigate the role of these bacteria, we assessed the development of colitis and extraintestinal manifestations in a mouse model in which colitis was induced in SCID mice by adoptive transfer of $CD4^+CD45RB^{high}$ T cells.

Materials and Methods

Mice

C57BL/6, BALB/c, C3HeJ, and CB17-icr SCID mice (6–8 wk old) were purchased from Japan CLEA (Tokyo, Japan). C57BL/6 RAG-$2^{-/-}$ mice

*Department of Gastroenterology and Hepatology, Graduate School, Tokyo Medical and Dental University, Tokyo 113-8510, Japan †Division of Gastroenterology and Hepatology, Department of Internal Medicine, Keio University School of Medicine, Tokyo 160-8582, Japan ‡Department of Gastroenterology and Hepatology, Okayama University Graduate School of Medicine, Dentistry and Pharmaceutical Sciences, Okayama City, Okayama 700-8558, Japan; and §Yakult Central Institute for Microbiological Research, Kunitachi, Tokyo 186-8650, Japan

Received for publication October 24, 2012. Accepted for publication April 8, 2013.

This study was supported in part by grants-in-aid for Scientific Research, Scientific Research on Priority Areas, Exploratory Research and Creative Scientific Research from the Japanese Ministry of Education, Culture, Sports, Science, and Technology; the Japanese Ministry of Health, Labour, and Welfare; the Japan Medical Association; the Foundation for Advancement of International Science; the Terumo Life Science Foundation; the Ohyama Health Foundation; the Yakult Bio-Science Foundation; the research fund of the Mitsukoshi Health and Welfare Foundation; Japan Foundation for Applied Enzymology; Kanae Foundation for the Promotion of Medical Science; and the Japanese Society of Gastroenterology.

Address correspondence and reprint requests to Dr. Mamoru Watanabe, Department of Gastroenterology and Hepatology, Graduate School, Tokyo Medical and Dental University, Tokyo 113-8510, Japan. E-mail address: mamoru.gast@tmd.ac.jp

The online version of this article contains supplemental material.

Abbreviations used in this article: ABX, antibiotics; CBA, cecal bacterial Ag; GF, germ-free; IBD, inflammatory bowel disease; IP, interstitial pneumonia; LP, lamina propria; MLN, mesenteric lymph node; MP, memory–phenotype; SP, spleen; SPF, specific pathogen-free; T_{EM}, effector–memory T; Treg, regulatory T; WT, wild-type.

www.jimmunol.org/cgi/doi/10.4049/jimmunol.1202930

were obtained from Taconic Farms (Hudson, NY) and Central Laboratories for Experimental Animals (Kawasaki, Japan). IL-$2^{-/-}$ mice were obtained from The Jackson Laboratory (Bar Harbor, ME). Specific pathogen-free (SPF) and GF breeding colonies of C3HeJ-SCID mice were established and maintained at the Animal Facilities (SPF) and the Gnotobiotic Facilities (GF) of Yakult Central Institute for Microbiological Research (Kunitachi, Tokyo). Sterility in the Gnotobiotic Facilities was tested monthly by culturing of feces and bedding as well as gram staining. RORγt-GFP reporter mice were provided by Dr. D. R. Littman (Departments of Microbiology and Pathology, New York University School of Medicine, New York, NY). The experimental protocols were approved by the Institutional Committees on Animal Research at the Tokyo Medical and Dental University and the Yakult Central Institute, and the experiments were approved by the regional animal study committees and were performed according to institutional guidelines and home office regulations.

Antibodies

The following mAbs were obtained from BD Pharmingen (San Diego, CA) and used to purify cell populations and for flow cytometric analysis: FITC-, PE-, PerCP-, and allophycocyanin-conjugated anti-mouse CD4 (RM4-5); FITC- and PerCP-conjugated anti-mouse CD3 (145-2C11); PE-conjugated anti-mouse CD44 (IM7); FITC-conjugated anti-mouse CD62L (MEL-14); PE-conjugated anti-mouse IL-17A; FITC-conjugated anti-mouse IFN-γ; PE-conjugated anti-mouse integrin-$\alpha_4\beta_7$ (DATK32); Alexa Fluor 647–conjugated anti-mouse CCR6; biotin-conjugated anti-rat CD29 (Ha2/5), which cross-reacts with mouse CD29; Alexa Fluor 647–conjugated anti-mouse CD49a (Ha31/8); FITC-conjugated anti-mouse CD69 (H1.2F3); FITC-conjugated anti-mouse CD45RB (16A); PE-conjugated anti-mouse CD25 (PC61); and PE-conjugated streptavidin. Biotin-conjugated anti-mouse IL-7Rα (A7R34) and PerCP-Cy5.5-conjugated anti-mouse CCR7 (4B12) were obtained from eBioscience (San Diego, CA).

Isolation of mononuclear cells from LP

The entire colon was opened longitudinally, washed with PBS, and cut into small pieces. The dissected mucosae were incubated in Ca^{2+}, Mg^{2+}-free HBSS containing 1 mM DTT (Sigma-Aldrich) for 30 min to remove mucus and incubated with 3 mg/ml collagenase A (Roche) for 2–3 h. The cells were subjected to Percoll (GE) density gradient centrifugation (40/75%).

Isolation of mononuclear cells from lung tissue

After reflux with PBS, the lungs were resected, washed with PBS, cut into small pieces, incubated with 3 mg/ml collagenase A (Roche) for 2–3 h, and subjected to Percoll (GE) density gradient centrifugation (40/75%).

Histological examination

Tissue samples were fixed in PBS containing 10% neutral-buffered formalin. Paraffin-embedded sections (5 μm) were stained with H&E. Two tissue samples from the proximal and distal parts of each colon were prepared and analyzed without prior knowledge of the type of T cell reconstitution or treatment. The area most affected in each colon was graded by the number and severity of lesions. The mean degree of inflammation in the colon was calculated as the sum of three parameters: crypt elongation, 0–3; mononuclear cell infiltration, 0–3; and frequency of crypt abscesses, 0–3 (6). The mean degree of inflammation in the lung was calculated using as the proportion of mononuclear cells infiltrating a lesion in the lung, with scores of 0, 1, 2, 3, 4, and 5 indicating 0, 10–30, 30–50, 50–80, and 80–100%, respectively (12).

Flow cytometry

Isolated spleen (SP), mesenteric lymph nodes (MLN), colonic LP, and lung cells were incubated with each Ab for 20 min on ice; cells stained with PerCP-Cy5.5–conjugated anti-mouse CCR7 were incubated with Ab for 30 min at room temperature and protected from light, as recommended by the manufacturer's protocol. The cells were subsequently analyzed by four-color FACSCalibur flow cytometry and CellQuest software (BD Biosciences, San Jose, CA).

Intracellular staining of cytokines

Isolated $CD4^+$ T cells were cultured for 12 h with ionomycin (500 ng/ml), PMA (50 ng/ml) and BD GolgiPlug (1 μl/ml; BD Pharmingen) and collected, and their surface molecules were stained. After cell fixation using a Cytofix/Cytoperm Kit (BD Pharmingen), the cells were stained with PE-conjugated anti–IL-17A mAb (TC11-18H10; BD Pharmingen) or FITC-conjugated anti-IFN-γ mAb (XMG1.2; BD Pharmingen) for 20 min.

Cytokine ELISA

To measure cytokine production, 3×10^4 $CD4^+$ T cells from LP were cultured in 200 ml culture medium at 37°C in a humidified atmosphere containing 5% CO_2 in 96-well plates (Costar, Cambridge, MA) precoated with 5 μg/ml hamster anti-mouse CD3e mAb (145-2C11; BD Pharmingen) and 2 μg/ml hamster anti-mouse CD28 mAb (37.51; BD Pharmingen) in PBS overnight at 4°C. After 48 h, the culture supernatants were removed, and cytokine concentrations were assayed using specific ELISA kits, as recommended by the manufacturer (R&D Systems, Minneapolis, MN).

Immunohistochemistry

Consecutive colon cryostat sections (5 μm) were fixed and stained with rat anti-mouse CD4 mAb (BD Pharmingen). After washing, the cells were incubated with 488 goat anti-hamster IgG (Molecular Probes). The cells were examined by fluorescence microscopy, using a BioZERO BZ8000 (Keyence, Tokyo, Japan). Staining of lung tissue with Masson–Trichrome stain was performed by Genostaff (Tokyo, Japan).

Induction of transfer colitis with $CD4^+CD45RB^{high}$ T cells

$CD4^+$ T cells were isolated from SPs of BALB/c or C3HeJ mice using the anti-CD4 (L3T4)-MACS system (Miltenyi Biotec, Auburn, CA), as recommended by the manufacturer. Enriched $CD4^+$ T cells were labeled with PE-conjugated anti-mouse CD4 and FITC-conjugated anti-mouse CD45RB, and $CD4^+CD45RB^{high}$ T cells were isolated using a FACSAria II. These cells were > 98% pure on reanalysis. Each SPF CB17-icr SCID or GF C3HeJ-SCID mouse was injected i.p. with 3×10^5 cells of these cells. The mice were weighed initially and then three times per week. They were also evaluated for clinical signs, such as hunched posture, piloerection, diarrhea, and blood in the stool. The mice were sacrificed 8 wk after transfer, and the clinical score of each was assessed as the sum of four parameters: hunching and wasting, 0 or 1; colon thickening, 0–3 (0, none; 1, mild; 2, moderate; and 3, extensive); and stool consistency, 0–3 (0, normal beaded stool; 1, soft stool; 2, diarrhea; and 3, bloody stool) (6).

In some experiments, SP $CD4^+$ T cells were labeled with FITC-conjugated anti-mouse CD4 and PE-conjugated anti mouse CD25. $CD4^+CD25^+$ T cells were isolated using a FACSAria II, and 3×10^5 $CD4^+CD25^+$ T cells were cotransferred with $CD4^+CD45RB^{high}$ T cells into SPF CB17-icr SCID mice as a negative control.

Antibiotics treatment

Some CB17-icr SCID mice were administered drinking water containing ampicillin (1 g/L), vancomycin (500 mg/l), neomycin sulfate (1 g/l), and metronidazole (1 g/l) 2 wk prior to beginning the adoptive transfer and during the course of the experiment. Control mice received drinking water without antibiotics.

Coculture of LP or lung $CD4^+$ T cells with APCs previously pulsed with cecal bacterial Ags

Cecal bacterial Ags (CBA) were prepared from colitic CB17-icr SCID mice previously transferred with $CD4^+CD45RB^{high}$ T cells. The cecum of each was opened, immersed in 1 ml PBS, and vortexed. DNAse (10 μg/ml) was added, and 1 ml of each suspension was added to 1 ml glass beads. The cells were disrupted at 5000 rpm in a Mini-Bead Beater (BioSpec Products, Bartlesville, OK) for 3 min and placed on ice. The glass beads and unlysed cells were removed by centrifuging at 5000 $\times$ *g* for 5 min. The lysates were filter-processed in a similar manner.

APCs were cocultured with $CD4^+$ T cells. SP cells from normal BALB/c mice were prepared, and 2×10^7 cells were incubated with 5 ml lysate solution in a 15-ml tube overnight at 37°C. These APCs were washed twice, treated with mitomycin *c*, and added to T cell cultures. LP and lung $CD4^+$ T cells obtained from normal mice and from colitic $CD4^+CD45RB^{high}$ T cell–transferred SCID mice were cultured in the presence of APCs pretreated with CBA in complete media. The culture supernatants were collected on day 3, and IFN-γ and IL-17 concentrations were assayed by ELISA.

Retransfer of LP $CD4^+$ T cells from colitic mice previously transferred with $ROR\gamma t^{GFP/+}CD4^+CD45RB^{high}$ T cells

Splenic $CD4^+CD45RB^{high}$ T cells from $ROR\gamma t^{GFP/+}$ mice were transferred into RAG-$2^{-/-}$ mice. Ten weeks later, the mice were sacrificed. LP $CD4^+$ T cells were isolated from colitic mice and $CD3^+CD4^+GFP^+$, $CD3^+CD4^+GFP^-$, and $CD3^+CD4^+$ populations were sorted by FACSAria II, and 3×10^5 cells were injected into each RAG-$2^{-/-}$ mouse.

Retransfer of lung T_{EM} cells into SCID mice

In the first experiment, CB17-icr SCID mice were pretreated with antibiotics. After 2 wk, they received 3×10^5 $CD4^+CD45RB^{high}$ T cells. Ten weeks later, these mice were sacrificed, and their lung $CD4^+$ T cells were isolated. $CD3^+CD4^+CD44^+CD62L^-$ T_{EM} cells were sorted by FACSAria II, and 3×10^5 of these cells were injected into each new CB17-icr SCID mouse, with or without pretreatment with antibiotics.

In the second experiment, GF C3HeJ SCID mice were injected with 3×10^5 $CD4^+CD45RB^{high}$ T cells. Ten weeks later, these mice were sacrificed, and lung $CD4^+$ T cells were isolated. $CD3^+CD4^+CD44^+CD62L^-$ cells were sorted with FACSAria II, and 3×10^5 of these cells were injected into each new GF or SPF C3HeJ SCID mouse.

Statistical analysis

Variables not normally distributed in either group were compared using the Mann–Whitney *U* test. If a variable was normally distributed in both groups, we assessed the variance within each group using the F test. If both groups were homoscedastic, between group differences were evaluated using Student *t* tests; if not, they were compared using Welch's *t* test. All statistical analyses were performed using Statcell software, with $p < 0.05$ defined as statistically significant.

Results

Antibiotics treatment prevents the development of colitis, but not pneumonitis, in SCID mice injected with $CD4^+CD45RB^{high}$ T cells

SCID mice injected with $CD4^+CD45RB^{high}$ T cells, alone or with T_R cells, were treated with a mixture of antibiotics (ABX) (vancomycin, neomycin, metronidazole, and ampicillin) or left untreated (Fig. 1A). Consistent with a previous report (7), SCID mice injected with $CD4^+CD45RB^{high}$ T cells without ABX treatment (hereafter called DW RB^{high} mice) rapidly developed severe wasting disease (Fig. 1Ba), with marked thickening of the colon wall (Fig. 1Bb). In contrast, mice injected with both $CD4^+CD45RB^{high}$ T cells and T_R cells without ABX treatment (DW RB^{high}/T_R mice) showed no wasting disease (Fig. 1Ba), and their colons appeared normal (Fig. 1Bb). Body weight loss differed significantly between these two groups (Fig. 1Ba). As expected, mice injected with $CD4^+CD45RB^{high}$ T cells, either alone or with $CD4^+CD25^+$ T_R cells, and treated with ABX (ABX RB^{high} and ABX RB^{high}/T_R, respectively) showed no evidence of wasting disease (Fig. 1Ba) with normal colon walls (Fig. 1Bb). Interestingly, ABX RB^{high} mice maintained body weight, whereas ABX RB^{high}/T_R mice gradually gained body weight, with their weights differing significantly 14 wk after transfer (Fig. 1B). Histological examination revealed that DW RB^{high} mice alone showed marked infiltration of mononuclear cells into the colonic LP (Fig. 1Ca) and a higher colitis score than the other three groups (Fig. 1Cb). The colitis scores of the ABX RB^{high} and ABX RB^{high}/T_R mice were comparable (Fig. 1Cb). Moreover, DW RB^{high} and ABX RB^{high} mice showed massive infiltration of mononuclear cells into the lungs, regardless of ABX treatment, whereas DW RB^{high}/T_R mice did not (Fig. 1Da). The interstitial pneumonia (IP) scores of mice that were and were not injected with T_R cells differed significantly (Fig. 1Db). Extraintestinal lesions in mice treated with ABX in the absence of T_R cells were specific to the lung, as we confirmed that other sites, including the thyroid, salivary glands, heart, stomach, small intestine, liver, kidneys, adrenal glands, ovaries, and joints, were almost normal in all groups of mice, even in the absence of T_R cells (data not shown).

Infiltration of $CD3^+CD4^+$ T cells was quantitatively evaluated by flow cytometry (Fig. 1E). The numbers of $CD3^+CD4^+$ T cells recovered from the colonic LP and MLNs of DW RB^{high} mice far exceeded the number originally injected, indicating extensive T cell proliferation and survival in the inflamed colons and MLNs of DW RB^{high} mice but not in the other three groups (Fig. 1E). In contrast, the absolute numbers of $CD3^+CD4^+$ T cells isolated from the lungs of DW RB^{high} and ABX RB^{high} mice were significantly higher than those from the lungs of DW RB^{high}/T_R and ABX RB^{high}/T_R mice (Fig. 1E). Immunohistochemical analysis revealed marked infiltration of $CD4^+$ T cells into the lungs of DW RB^{high} and ABX RB^{high} mice but not of DW RB^{high}/T_R and ABX RB^{high}/T_R mice (Fig. 1F).

The concentrations of IFN-γ and IL-17A secreted into the media by colonic LP $CD4^+$ T cells of DW RB^{high} mice was significantly higher than those of the other three groups (Fig. 1G). Consistent with the pathology of pneumonitis in the lungs of DW RB^{high} and ABX RB^{high} mice, the concentrations of IFN-γ and IL-17A secreted by their lung $CD4^+$ T cells were significantly higher than those of that of DW RB^{high}/T_R and ABX RB^{high}/T_R mice (Fig. 1G). Intriguingly, the production of IFN-γ by lung $CD4^+$ T cells of ABX RB^{high} mice was significantly lower than that of DW RB^{high} mice, whereas their production of IL-17A was comparable. Regardless of the presence or absence of T_R cells, and with or without ABX treatment, the cells recovered from the colon and lungs of these mice had the $CD44^{high}CD62L^-IL\text{-}7R\alpha^{high}$ T_{EM} cell phenotype (Supplemental Fig. 1A). Masson–Trichrome staining of the lung showed fibrosis, indicating chronic inflammation, in the lungs of ABX RB^{high} and DW RB^{high} mice, but no fibrosis in the lungs of ABX RB^{high}/T_R and DW RB^{high}/T_R mice (Supplemental Fig. 1B). Collectively, these results indicate that ABX modulation of intestinal microbiota suppresses the development of colitis but not extraintestinal pneumonitis, whereas T_R cells suppress the development of both conditions.

$IL\text{-}2^{-/-}$ mice developed both colitis and IP

To exclude the possibility that IP was specific to the SCID transfer model, we evaluated $IL\text{-}2^{-/-}$ mice, which spontaneously develop both autoimmune diseases and colitis because of T_R reduction. After they developed colitis, $IL\text{-}2^{-/-}$ mice were treated with ABX for 4 wk, resulting in the disappearance of colitis symptoms in all ABX-treated $IL\text{-}2^{-/-}$ mice. A comparison of age matched ABX-treated $IL\text{-}2^{-/-}$ mice (ABX $IL\text{-}2^{-/-}$), colitic $IL\text{-}2^{-/-}$ mice (DW $IL\text{-}2^{-/-}$), and C57BL/6J mice (wild type [WT]) showed that DW $IL\text{-}2^{-/-}$ mice developed severe colitis, ABX $IL\text{-}2^{-/-}$ mice developed very slight colitis, and control WT mice did not develop colitis (Supplemental Fig. 2A, 2B). Consistent with this finding, the absolute numbers of colonic LP $CD3^+CD4^+$ T cells were significantly higher in DW $IL\text{-}2^{-/-}$ than in ABX $IL\text{-}2^{-/-}$ and WT mice (Supplemental Fig. 2C). We also found that large numbers of mononuclear cells had infiltrated the lung interstitial lesions of both DW $IL\text{-}2^{-/-}$ and ABX $IL\text{-}2^{-/-}$ mice but not of WT mice (Supplemental Fig. 2D). IP scores and the absolute number of lung $CD3^+CD4^+$ cells were significantly higher in DW $IL\text{-}2^{-/-}$ and ABX $IL\text{-}2^{-/-}$ mice than in WT mice (Supplemental Fig. 2E, 2F), confirming that $IL\text{-}2^{-/-}$ mice also developed T cell–mediated IP regardless of ABX treatment. Intracellular staining of cytokines revealed that colonic LP and lung $CD4^+$ T cells of $IL\text{-}2^{-/-}$ mice were abundant in Th1, Th17/Th1, and Th17 subpopulations (Supplemental Fig. 2G).

Infiltrating lung $CD4^+$ T cells in colitic mice produce IFN-γ and IL-17A in response to cecal bacterial Ags

Because DW RB^{high} and ABX RB^{high} mice developed IP, with marked infiltration of Th17 and Th1 T_{EM} cells in the lungs, we assessed whether these colitic lung $CD4^+$ T cells could respond to Ags derived from commensal bacteria (CBA) by synthesizing and secreting IFN-γ and IL-17A in vitro. Significantly higher levels of IFN-γ and IL-17A were produced by colitic LP and lung $CD4^+$ T cells in response to CBA than by normal colonic LP and lung